

Towards Open World Active Learning for 3D Object Detection

Zhuoxiao Chen · Yadan Luo · Zixin Wang · Zijian Wang · Xin Yu · Zi Huang

Received: date / Accepted: date

Abstract Significant strides have been made in closed-world 3D object detection, testing systems in environments with known classes. However, the challenge arises in open world scenarios where new object classes appear. Existing efforts sequentially learn novel classes from streams of labeled data at a significant annotation cost, impeding efficient deployment to the wild. To seek effective solutions, we investigate a more practical yet challenging research task: Open World Active Learning for 3D Object Detection (OWAL-3D), aiming at selecting a small number of 3D boxes to annotate while maximizing detection performance on both known and unknown classes. The core difficulty centers on striking a balance between mining more unknown instances and minimizing the labeling expenses of point clouds. Empirically, our study finds the harmonious and inverse relationship between box quantities and their confidences can help alleviate the dilemma, avoiding the repeated selection of common known instances and focusing on uncertain objects that are potentially unknown. We unify both relational constraints into a simple and effective AL strategy namely Open-CRB, which guides to acquisition of informative point clouds with the least amount of boxes to label. Furthermore, we develop a comprehensive codebase for easy reproducing and future research, supporting 15 baseline methods (*i.e.*, active learning, out-of-distribution detection and open world detection), 2 types of modern 3D detectors (*i.e.*, one-stage SECOND and two-stage PV-RCNN) and 3 benchmark 3D datasets (*i.e.*, KITTI, nuScenes and Waymo). Extensive experiments evidence

that the proposed Open-CRB demonstrates superiority and flexibility in recognizing both novel and shared categories with very limited labeling costs, compared to state-of-the-art baselines.

Keywords Open World Object Detection, Active Learning, 3D Object Detection

1 Introduction

3D object detection based on LiDAR technology is essential for understanding complex 3D scenes in various fields, including autonomous driving (Wang et al 2020; Deng et al 2021; Qian et al 2022; Chen et al 2023) and robotics (Ahmed et al 2018; Wang et al 2019; Montes et al 2020). Conventional 3D object detection methodologies typically assume the test data shares the same class set as the training data, referred to as Closed World 3D Object Detection (CW-3OD). Nevertheless, in the practical deployment of 3D object detectors, this assumption does not always hold true, as a stream of novel/unknown categories constantly arises in the real-world environment. Thus, contemporary object detection models are required to identify and learn those instances of unknown categories, referred to as Open World Object Detection (OW-OD) (Joseph et al 2021). However, it is non-trivial to extend existing CW-3OD approaches to the open world due to a lack of knowledge about novel classes, rendering the failure of traditional detection methods. For example, if a 3D detector was trained with *pedestrian* class only, it is likely to miss-classify similar-shape objects as pedestrians with high confidence (*e.g.*, bike rack with 0.86 confidence, signboard with 0.74 confidence) (Huang et al 2022), or miss-detect dissimilar-shape objects as shown in Figure 1. This misclassification can precipitate erroneous

School of Electrical Engineering and Computer Science
The University of Queensland, Australia
E-mail: {zhuoxiao.chen, y.luo, zixin.wang, zijian.wang, xin.yu, helen.huang}@uq.edu.au

decision-making by systems, engendering safety concerns of autonomous driving cars. Consequently, there is an urgent need to develop algorithms that help identify unknown/novel categories within point clouds in the open world environments.

To this end, recent works has rapidly shifted their focus to the OW-OD task, while two main challenges were encountered (Wu et al 2022b; Yu et al 2022): detection models may 1) miss-detect objects of novel class, 2) misclassify novel classes to known. Efforts have aimed to either enhance the proposal localization for unknown objects (Ma et al 2023b) or learn a better embedding to distinguish known and unknown instances (Maaz et al 2022), to tackle these two challenges, respectively. While the commonness shared by these OW-OD methods is shown in Figure 1, they leverage a continual learning paradigm to initially acquire a sufficient number of point clouds with some specific classes manually annotated, to train the detection model. Subsequently, this iterative process is repeated in multiple rounds to incorporate additional novel classes. Although, these endeavors have proven successful in recognizing unknown classes, nevertheless, all of them are required to train their models using substantial volumes of data manually labeled by human annotators in each round. When a significant volume of fresh data arrives, manually labeling new categories within it becomes very time-consuming and costly. This challenge is especially pronounced in the case of 3D object detection, where precisely labeling a single 3D bounding box necessitates 7-degree of freedom (DOF) encompassing position, size, and orientation data and demands over 100 seconds for an annotator (Song et al 2015). Such prerequisite for grasping new category knowledge significantly impedes the practicality and efficiency of implementing these OW-OD methodologies in practice, especially when the annotation budget is limited.

To overcome this constraint, Active Learning (AL) proves valuable by selectively querying labels for a small fraction from a large pool of unlabeled data. The objective of AL selection criterion is to quantify the sample informativeness, using the heuristics derived from *sample uncertainty* (Gal et al 2017; Du et al 2021; Caramalau et al 2021; Yuan et al 2021; Choi et al 2021; Zhang et al 2020; Shi and Li 2019) and *sample diversity* (Ma et al 2021; Gudovskiy et al 2020; Gao et al 2020; Sinha et al 2019; Pinsler et al 2019). In particular, uncertainty-driven approaches focus on the samples that the model is the least confident of their labels, thus searching for the candidates with: maximum entropy (MacKay 1992; Shannon 1948; Kim et al 2021b; Siddiqui et al 2020; Shi and Yu 2019), disagreement among different experts (Freund et al 1992; Tran

et al 2019), minimum posterior probability of a predicted class (Wang et al 2017), or the samples with reducible yet maximum estimated error (Roy and McCallum 2001b; Yoo and Kweon 2019; Kim et al 2021a). On the other hand, diversity-based methods try to find the most representative samples to avoid sample redundancy. To this end, they form subsets that are sufficiently diverse to describe the entire data pool by making use of the greedy coresets algorithms (Sener and Savarese 2018), or the clustering algorithms (Nguyen and Smeulders 2004). Recent works (Liu et al 2021; Citovsky et al 2021; Kirsch et al 2019; Houlsby et al 2011) combine the aforementioned heuristics: they measure uncertainty as the gradient magnitude of samples (Ash et al 2020) or its second-order metrics (Liu et al 2021) at the final layer of neural networks, and then select samples with gradients spanning a diverse set of directions. Another stream of works apply active learning to 2D/3D object detection tasks (Feng et al 2019; Schmidt et al 2020; Wang et al 2022; Wu et al 2022a; Tang et al 2021b), by leveraging ensemble (Beluch et al 2018) or Monte Carlo (MC) dropout (Gal and Ghahramani 2016) algorithms to estimate the classification and localization uncertainty of bounding boxes for images/-point clouds acquisition. However, these existing AL methods are not guaranteed to identify and select sufficient novel instances when the pool of unlabeled data includes unknown categories. Such limitation may impede the existing active learning algorithms from being employed in the open world.

To investigate whether active learning has the capacity to discover novel classes, in this paper, we propose a novel and practical task: Open World Active Learning for 3D Object Detection (OWAL-3D). Specifically, given a 3D object detector pre-trained with known class only, and a large pool of unlabeled point clouds that contain novel classes of interest, the objective of OWAL-3D is to query informative point clouds at every selection round. As illustrated in Figure 1, these chosen point clouds are annotated by oracle then train the 3D detectors, aiming to maximize the detection model performance on both unknown and known, all the while minimizing the associated annotation costs (*i.e.*, minimize the number of the annotated bounding box). In this paper, to comprehensively explore OWAL-3D, as well as to make it more easily reproducible and reused for future work, we build up a large-scale and open-sourced benchmark integrating existing approaches of AL, out-of-distribution detection (OOD) and OW-OD, with commonly used 3D detection datasets and backbone models. However, during the investigation, 2 major research questions of OWAL-3D are encountered:

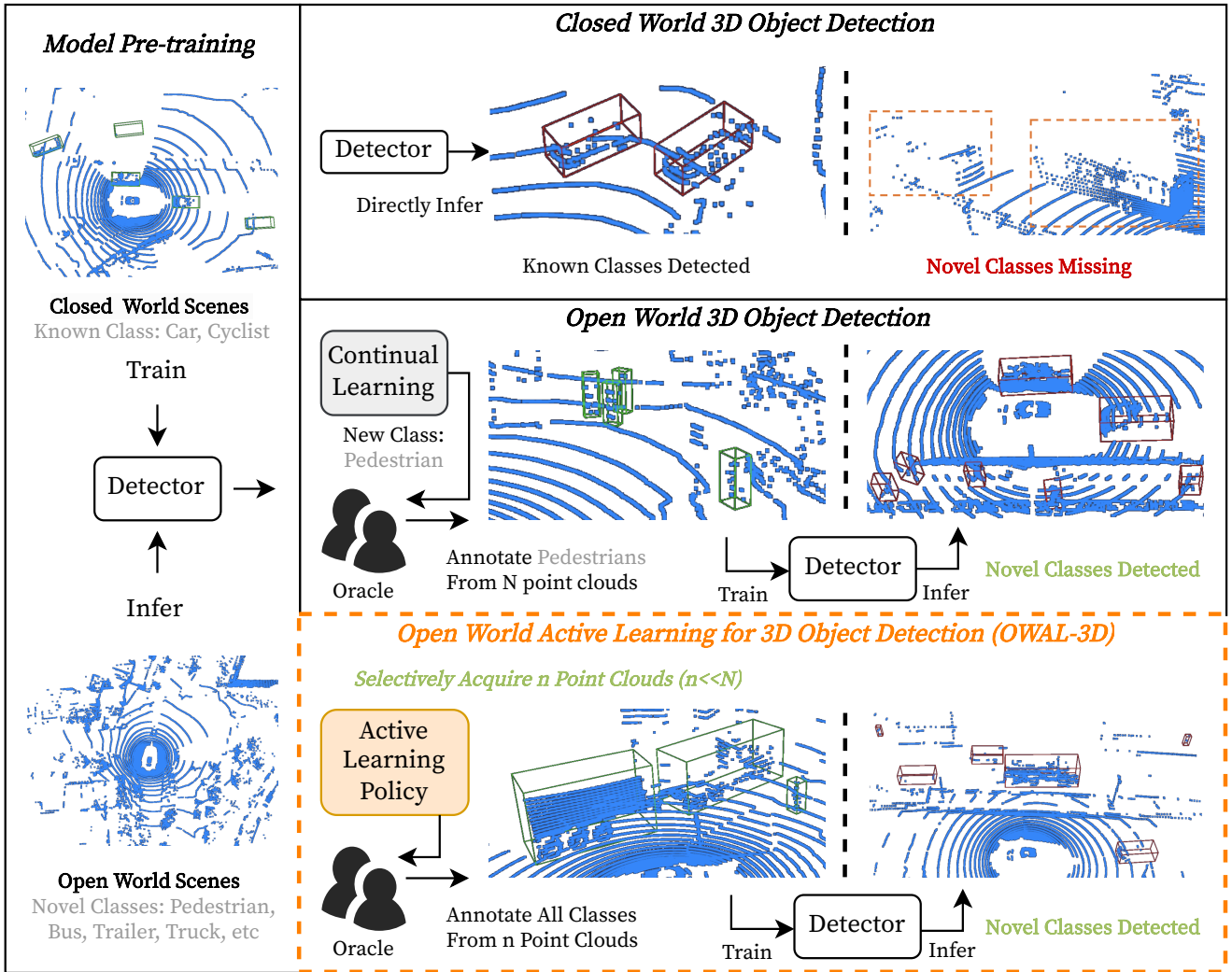


Fig. 1: An illustrative flowchart of the proposed Open World Active Learning for 3D Object Detection (OWAL-3D) and conventional tasks. Given a pre-trained 3D detector, traditional closed world 3D detection methods struggle to localize and recognize objects of new classes in an open world context, as shown in the upper case. While, open world 3D object detection (middle case) incorporates the strategy of continual learning (Joseph et al 2021), which enables the model to learn specific novel categories extensively labeled by human annotators. To save labeling resources and time, we introduce OWAL-3D, as shown in the lower case, to selectively acquire and label a small portion of point clouds from the open world utilizing an Active Learning (AL) policy. AL method allows the 3D detection model to efficiently generalize to new scenes containing novel object categories, with saved time and expense.

1. How can AL select point clouds that are likely to contain novel/unknown classes?
2. How to balance the trade-offs between annotation cost and detection performance?

To answer Question 1, we empirically notice uncertainty-based methods at the first selection round tend to mine more unknown instances. This finding motivates us to seek unknowns from the perspective of instance uncertainty. However, existing methods were originally devised to enhance and assess the uncertainty at sample-

level, but do not account for the amounts of instances within each sample (*i.e.*, number of objects within images or point clouds). Consequently, relying on these algorithms for selecting point clouds is likely to increase labeling costs, given that point clouds containing a greater number of objects are more likely to contain uncertain objects. This dilemma leads us to Question 2, which was already encountered in our preliminary study CRB (Luo et al 2023b). In CRB, a label conciseness (LC) criterion was proposed to measure the con-

ciseness and diversity of labels within each point cloud. It first counts the number of predicted boxes for each label and then computes entropy based on the distribution of each label. The higher entropy score indicates the predicted labels are more diverse and concise in the point clouds. Also, LC reveals that label diversity is a useful indicator of point clouds that well trade-off between a number of bounding boxes and model performance. While effective, this criterion is based entirely on predicted known labels and, thus cannot be readily applied to the realm of open world scenarios.

In response to the aforementioned challenges, our approach extends the label conciseness from the preliminary study (Luo et al 2023b) to simple and effective selection criteria: Open Label Conciseness (OLC), tailed for mining point clouds with a higher likelihood of containing novel classes under the open world environment. Meanwhile, OLC strikes an equilibrium between unknown instances of exploitation and saving annotation costs. Specifically, based on answers to Question 1 (*i.e.*, uncertainty matters), we replace the conventional hard label predictions of known categories with soft labels (*i.e.*, prediction confidence) to more accurately reflect the component of known labels within the point cloud. More importantly, the component of unknown labels then can be estimated by computing the sum of differences between hard labels and soft labels across all predicted bounding boxes within each point cloud. Finally, the open label conciseness is simply computing the entropy of soft box labels and estimated unknown labels. This strategy can be mathematically interpreted into two relationships: (1) harmonic relationship of confidences across different classes, (2) inverse relationship between the number of boxes and their respective confidences. The former secures a diverse and concise set of categories within selected point clouds, while the latter actively seeks out more boxes with lower prediction confidence, helping the discovery of novel categories. The two relationships mutually constrain each other to adequately address the two primary challenges posed in OWAL-3D tasks, respectively. Compared to the label conciseness criteria in a preliminary study, we invoke refined known components and further estimate unknown label components, resulting in conciseness for both labels.

The empirical study suggests the significance of the initial phase of active selection. Acquiring labels for the majority of unknown instances in the first round simplifies the subsequent selection process as CWAL-3D. According to the finding, we choose point clouds with the top K entropy calculated by OLC to enable 3D detection model to swiftly generalize to all novel categories. Then the task shifts to a closed world scenario as the

model already acquired knowledge of novel classes. In subsequent active selection rounds, we revert to CRB for point cloud acquisition. The ultimate framework, Open-CRB, seamlessly integrates OLC and CRB, allowing it to be dynamically applicable to both closed world and open world scenarios.

A preliminary version of this work was presented in (Luo et al 2023b). In this work, we additionally (1) introduce a more realistic setting: Open World Active Learning for 3D Object Detection (OWAL-3D), aiming to efficiently generalize 3D detection models to any open world environments, through training on a very small proportion of point clouds selected by active learning policy. (2) We introduce a novel variant Open-CRB framework tailored for saving annotation cost and maximizing the model performance on both novel and shared categories. (3) We conduct extensive experiments for the proposed Open-CRB approach and recent baselines to two 3D object detection datasets, KITTI and nuScenes. The proposed Open-CRB achieves state-of-the-art performance in both novel classes and shared classes, with the least number of annotated bounding boxes, compared to conventional active learning, out-of-distribution detection, and open world object detection methods. (4) We have developed a large-scale and open-source codebase for both OWAL-3D and Closed World Active Learning for 3D Object Detection (CWAL-3D), incorporating 15 baselines, 3 benchmark datasets and 2 supported modern 3D detectors. This robust codebase can be utilized for easily reproducing results and facilitating future researchers in this field.

2 Related Work

2.1 Active Learning

For a comprehensive review of classic active learning methods and their applications, we refer readers to (Ren et al 2021). Most active learning approaches were tailored for image classification task, where the *uncertainty* (Wang and Shang 2014; Lewis and Catlett 1994; Joshi et al 2009; Roth and Small 2006; Parvaneh et al 2022; Du et al 2021; Kim et al 2021b; Bhatnagar et al 2021) and *diversity* (Sener and Savarese 2018; Elhamifar et al 2013; Guo 2010; Yang et al 2015; Nguyen and Smeulders 2004; Hasan and Roy-Chowdhury 2015; Aodha et al 2014) of samples are measured as the acquisition criteria. The hybrid works (Kim et al 2021a; Citovsky et al 2021; Ash et al 2020; MacKay 1992; Liu et al 2021; Kirsch et al 2019; Housby et al 2011) combine both paradigms such as by measuring uncertainty as to the gradient magnitude (Ash et al 2020) at the final layer of neural networks and selecting gradients that

span a diverse set of directions. In addition to the above two mainstream methods, (Settles et al 2007; Roy and McCallum 2001a; Freytag et al 2014; Yoo and Kweon 2019) estimate the expected model changes or predicted losses as the sample importance.

2.2 Active Learning for Object Detection

Lately, the attention of AL has shifted from image classification to the task of object detection (Siddiqui et al 2020; Li and Yin 2020). Early work (Roy et al 2018) exploits the detection inconsistency of outputs among different convolution layers and leverages the query by committee approach to select informative samples. Concurrent work (Kao et al 2018) introduces the notion of localization tightness as the regression uncertainty, which is calculated by the overlapping area between region proposals and the final predictions of bounding boxes. Other uncertainty-based methods attempt to aggregate pixel-level scores for each image (Aghdam et al 2019), reformulate detectors by adding Bayesian inference to estimate the uncertainty (Harakeh et al 2020) or replace conventional detection head with the Gaussian mixture model to compute aleatoric and epistemic uncertainty (Choi et al 2021). A hybrid method (Wu et al 2022a) considers image-level uncertainty calculated by entropy and instance-level diversity measured by the similarity to the prototypes. Lately, AL technique is leveraged for transfer learning by selecting a few uncertain labeled source bounding boxes with high transferability to the target domain, where the transferability is defined by domain discriminators (Tang et al 2021b; Al-Saffar et al 2021). Inspired by neural architecture searching, Tang et al (2021a) adopted the ‘swap-expand’ strategy to seek a suitable neural architecture including depth, resolution, and receptive fields at each active selection round. Recently, some works augment the Weakly-Supervised Object Detection (WS-OD) with an active learning scheme. In WS-OD, only image-level category labels are available during training. Some conventional AL methods such as predicted probability, probability margin are explored in (Wang et al 2022), while in (Vo et al 2022), “box-in-box” is introduced to select images where two predicted boxes belong to the same category and the small one is “contained” in the larger one. Nevertheless, it is not trivial to adapt all existing AL approaches for 2D detection as the ensemble learning and network modification leads to more model parameters to learn, which could be hardly affordable for 3D tasks.

Active learning for 3D object detection has been relatively under-explored than other tasks, potentially due to its large-scale nature. Most existing works (Feng et al

2019; Schmidt et al 2020) simply apply the off-the-shelf generic AL strategies and use hand-crafted heuristics including Shannon entropy (Wang and Shang 2014), ensemble (Beluch et al 2018), localization tightness (Kao et al 2018), Mc-dropout (Gal and Ghahramani 2016) and neural tangent kernel (Luo et al 2023a) for 3D detection learning. However, the abovementioned solutions base on the cost of labelling point clouds rather than the number of 3D bounding boxes, which inherently being biased to the point clouds containing more objects. However, in our work, the proposed CRB greedily search for the unique point clouds while maintaining the same marginal distribution for generalization, which implicitly quires objects to annotate without repetition and save labeling costs.

2.3 Open World Object Detection

The Open World Object Detection (OWAD) task, introduced recently in the work of Joseph et al (2021), has garnered considerable attention within the research community, owing to its potential real-world applications. Joseph et al (2021) propose an ORE approach that enhances the faster-RCNN model’s ability to recognize and learn unknown objects, by feature-space contrastive clustering, an RPN-based unknown object detector, and an Energy-Based Unknown Identifier. Building upon the ORE, Yu et al (2022) further extended the methodology by addressing the issue of distribution overlap between known and unknown classes in feature space embeddings, reducing the confusion that often arises when distinguishing between known and unknown objects. Simultaneously, Wu et al (2022b) endeavored to extend ORE by introducing an additional objectiveness detection head that predicts the Intersection over Union (IoU) between the localized bounding boxes and the corresponding ground truth boxes. In an effort to refine the decision boundaries of known and unknown classes, Ma et al (2023b) propose to decouple the known and unknown features, thus promoting both known and unknown object recognition.

In recent times, there has been a notable surge in the adaptation of transformer-based techniques in the context of Open World Object Detection (OW-OD). The pioneering work by Gupta et al (2022) introduced OW-DETR, an adaptation of the Deformable DETR model tailored to confront the specific challenges posed by OW-OD tasks. OW-DETR leverages a pseudo-labeling approach to supervise the detection of unknown objects, wherein unmatched object proposals with strong backbone activations are characterized as potential unknown objects. Seeking to enhance the localization capabilities of transformer-based object detectors, Maaz

et al (2022) developed Multi-modal Vision Transformers (MViT) to align image-text pairs. Since textual language descriptions convey high-level information, the fusion of modalities aids learning fairly generalizable properties of universal object categories. Different from MViT, which relies on language modality to improve the model, PROB (Zohar et al 2023) integrates probabilistic models into existing OW-DETR framework to facilitate objectiveness estimation within the embedded feature space. Furthermore, an evolution of the OW-DETR model is presented in the form of the LoCalization and IdentificAtion Cascade Detection Transformer (CAT) by Ma et al. (Ma et al 2023a). CAT aims to emulate human thinking patterns, which inherently prioritizes the initial detection of all foreground objects before delving into detailed recognition. To achieve this, CAT decouples the detection process in the cascade decoding way to prioritize localization before classification, enhancing the model’s capacity to identify and retrieve unknown objects in open world environments.

However, current OW-OD techniques suffer from the drawback of requiring extensive manual annotations to facilitate the detection model in learning new classes, hindering the efficient deployment of the model in open-world environments. In this study, we employ active learning to address this issue. By acquiring a small subset of samples for training, generalization to open world scenarios becomes not only more cost-effective but also quicker compared to traditional OW-OD methods.

3 Preliminaries

In this section, we introduce the notations, problem settings, definitions, and theoretical analysis for the tasks of Closed World Active Learning for 3D Object Detection (CWAL-3D).

3.1 Problem Definition of CWAL-3D

In this section, we mathematically formulate the problem of active learning for 3D object detection and set up the notations.

Definition 1 (3D Object Detection) Given an orderless LiDAR point cloud $\mathcal{P} = \{x, y, z, e\}$ with 3D location (x, y, z) and reflectance e , the goal of 3D object detection is to localize the objects of interest as a set of 3D bounding boxes $\mathcal{B} = \{b_k\}_{k \in [N_B]}$ with N_B indicating the number of detected bounding boxes, and predict the associated box labels $Y = \{y_k\}_{k \in [N_B]} \in \mathcal{Y} = \{1, \dots, C\}$, with C being the number of classes to predict.

Each bounding box b represents the relative center position (p_x, p_y, p_z) to the object ground planes, the

box size (l, w, h) , and the heading angle θ . Mainstream 3D object detectors use point clouds \mathcal{P} to extract point-level features $\mathbf{x} \in \mathbb{R}^{W \cdot L \cdot F}$ (Shi et al 2019; Yang et al 2019, 2020) or by voxelization (Shi et al 2020), with W, L, F representing width, length, and channels of the feature map. The feature map \mathbf{x} is passed to a classifier $f(\cdot; \mathbf{w}_f)$ parameterized by \mathbf{w}_f and regression heads $g(\cdot; \mathbf{w}_g)$ (e.g., box refinement and ROI regression) parameterized by \mathbf{w}_g . The output of the model is the detected bounding boxes $\hat{\mathcal{B}} = \{\hat{b}_k\}$ with the associated box labels $\hat{Y} = \{\hat{y}_k\}$ from anchored areas. The loss functions ℓ^{cls} and ℓ^{reg} for classification (e.g., regularized cross entropy loss Oberman and Calder (2018)) and regression (e.g., mean absolute error/ L_1 regularization Qi et al (2020)) are assumed to be Lipschitz continuous.

Definition 2 (CWAL-3D) In an active learning pipeline, a small set of labeled point clouds $\mathcal{D}_L = \{(\mathcal{P}, \mathcal{B}, Y)_i\}_{i \in [m]}$ and a large pool of raw point clouds $\mathcal{D}_U = \{(\mathcal{P})_j\}_{j \in [n]}$ are provided at training time, with n and m being a total number of point clouds and $m \ll n$. For each active learning round $r \in [R]$, and based on the criterion defined by an active learning policy, we select a subset of raw data $\{\mathcal{P}_j\}_{j \in [N_r]}$ from \mathcal{D}_U and query the labels of 3D bounding boxes from an oracle $\Omega : \mathcal{P} \rightarrow \mathcal{B} \times \mathcal{Y}$ to construct $\mathcal{D}_S = \{(\mathcal{P}, \mathcal{B}, Y)_j\}_{j \in [N_r]}$. The 3D detection model is pre-trained with \mathcal{D}_L for active selection, and then retrained with $\mathcal{D}_S \cup \mathcal{D}_L$ until the selected samples reach the final budget B , i.e., $\sum_{r=1}^R N_r = B$.

3.2 CWAL-3D: Motivation

Theoretical Motivation of CRB. The core question of active learning for 3D detection is how to design a proper criterion, based on which a fixed number of unlabeled point clouds can be selected to achieve minimum empirical risk $\mathfrak{R}_T[\ell(f, g; \mathbf{w})]$ on the test set \mathcal{D}_T and minimum annotation time. Below, inspired by (Mansour et al 2009; Ben-David et al 2010), we derive the following **generalization bound** for active learning for 3D detection so that the desired acquisition criteria can be obtained by optimizing the generalization risk.

Theorem 1 Let \mathcal{H} be a hypothesis space of Vapnik-Chervonenkis (VC) dimension d , with f and g being the classification and regression branches, respectively. The $\hat{\mathcal{D}}_S$ and $\hat{\mathcal{D}}_T$ represent the empirical distribution induced by samples drawn from the acquired subset \mathcal{D}_S and the test set \mathcal{D}_T , and ℓ the loss function bounded by \mathcal{J} . It is proven that $\forall \delta \in (0, 1)$, and $\forall f, g \in \mathcal{H}$, with probability

at least $1 - \delta$ the following inequality holds,

$$\mathfrak{R}_T[\ell(f, g; \mathbf{w})] \leq \mathfrak{R}_S[\ell(f, g; \mathbf{w})] + \frac{1}{2} \text{disc}(\widehat{\mathcal{D}}_S, \widehat{\mathcal{D}}_T) + \lambda^* + \text{const},$$

$$\text{where const} = 3\mathcal{J}\left(\sqrt{\frac{\log \frac{4}{\delta}}{2N_r}} + \sqrt{\frac{\log \frac{4}{\delta}}{2N_t}}\right) + \sqrt{\frac{2d \log(eN_r/d)}{N_r}} + \sqrt{\frac{2d \log(eN_t/d)}{N_t}}.$$

Notably, $\lambda^* = \mathfrak{R}_T[\ell(f^*, g^*; \mathbf{w}^*)] + \mathfrak{R}_S[\ell(f^*, g^*; \mathbf{w}^*)]$ denotes the joint risk of the optimal hypothesis f^* and g^* , with \mathbf{w}^* being the model weights. N_r and N_t indicate the number of samples in the \mathcal{D}_S and \mathcal{D}_T . The proof can be found in (Luo et al 2023b).

Remark 1 The first term indicates the training error on the selected subsets, which is assumed to be trivial based on the zero training assumption (Sener and Savarese 2018). To obtain a tight upper bound of the generalization risk, the **optimal subset** \mathcal{D}_S^* can be determined via minimizing the discrepancy distance of empirical distribution of two sets, *i.e.*,

$$\mathcal{D}_S^* = \arg \min_{\mathcal{D}_S \subset \mathcal{D}_U} \text{disc}(\widehat{\mathcal{D}}_S, \widehat{\mathcal{D}}_T).$$

Below, we define the discrepancy distance for the 3D object detection task.

Definition 3 (Distribution Discrepancy) For any $f, g, f', g' \in \mathcal{H}$, the discrepancy between the distribution of the selected sets \mathcal{D}_S and unlabeled pool \mathcal{D}_T can be formulated as,

$$\text{disc}(\widehat{\mathcal{D}}_S, \widehat{\mathcal{D}}_T) = \sup_{f, f' \in \mathcal{H}} |\mathbb{E}_{\widehat{\mathcal{D}}_S} \ell(f, f') - \mathbb{E}_{\widehat{\mathcal{D}}_T} \ell(f, f')| + \sup_{g, g' \in \mathcal{H}} |\mathbb{E}_{\widehat{\mathcal{D}}_S} \ell(g, g') - \mathbb{E}_{\widehat{\mathcal{D}}_T} \ell(g, g')|,$$

where the bounded expected loss ℓ for any classification and regression functions are symmetric and satisfy the triangle inequality.

Remark 2 As 3D object detection is naturally an integration of classification and regression tasks, mitigating the set discrepancy is basically aligning the inputs and outputs of each branch. Therefore, with the detector frozen during the active selection, finding an optimal \mathcal{D}_S^* can be interpreted as enhancing the acquired set's (1) **Label Conciseness**: aligning marginal label distribution of bounding boxes, (2) **Feature Representativeness**: aligning marginal distribution of the latent representations of point clouds, and (3) **Geometric Balance**: aligning marginal distribution of geometric

characteristics of point clouds and predicted bounding boxes, and can be written as:

$$\mathcal{D}_S^* \approx \arg \min_{\mathcal{D}_S \subset \mathcal{D}_U} \underbrace{d_{\mathcal{A}}(P_{\widehat{Y}_S}, P_{Y_T})}_{\text{Conciseness}} + \underbrace{d_{\mathcal{A}}(P_{X_S}, P_{X_T})}_{\text{Representativeness}} + \underbrace{d_{\mathcal{A}}(P_{\phi(\mathcal{P}_S, \widehat{\mathcal{B}}_S)}, P_{\phi(\mathcal{P}_T, \mathcal{B}_T)})}_{\text{Balance}}. \quad (1)$$

Here, \mathcal{P}_S and \mathcal{P}_T represent the point clouds in the selected set and the ones in the test set. $\phi(\cdot)$ indicates the geometric descriptor of point clouds and $d_{\mathcal{A}}$ distance (Kifer et al 2004) which can be estimated by a finite set of samples. For latent features X_S and X_T , we only focus on the features that differ from the training sets, since $\mathbb{E}_{\widehat{\mathcal{D}}_L} \ell^{cls} = 0$ and $\mathbb{E}_{\widehat{\mathcal{D}}_L} \ell^{reg} = 0$ based on the zero training error assumption. Considering that test samples and their associated labels are not observable during training, we make an assumption on the prior distributions of test data. WLOG, we assume that the prior distribution of bounding box labels and geometric features are uniform. Note that we can adopt the KL-divergence for the implementation of $d_{\mathcal{A}}$ assuming that latent representations follow the univariate Gaussian distribution.

Connections with existing AL approaches. The proposed criteria jointly optimize the discrepancy distance for both tasks with three objectives, which shows the connections with existing AL strategies. The uncertainty based methods focus strongly on the first term, based on the assumption that learning more difficult samples will help to improve the suprema of the loss. This rigorous assumption can result in a bias towards hard samples, which will be accumulated and amplified across iterations. Diversity-based methods put more effort into minimizing the second term, aiming to align the distributions in the latent subspace. However, the diversity-based approaches are unable to discover the latent features specified for regression, which can be critical when dealing with a detection problem. We introduce the third term for the 3D detection task, motivated by the fact that aligning the geometric characteristics of point clouds helps to preserve the fine-grained details of objects, leading to more accurate regression.

3.3 CWAL Approach: CRB

To optimize the three criteria outlined in Eq. 2, we derive an AL scheme consisting of three components. In particular, to reduce the computational overhead, we hierarchically filter the samples that meet the selection

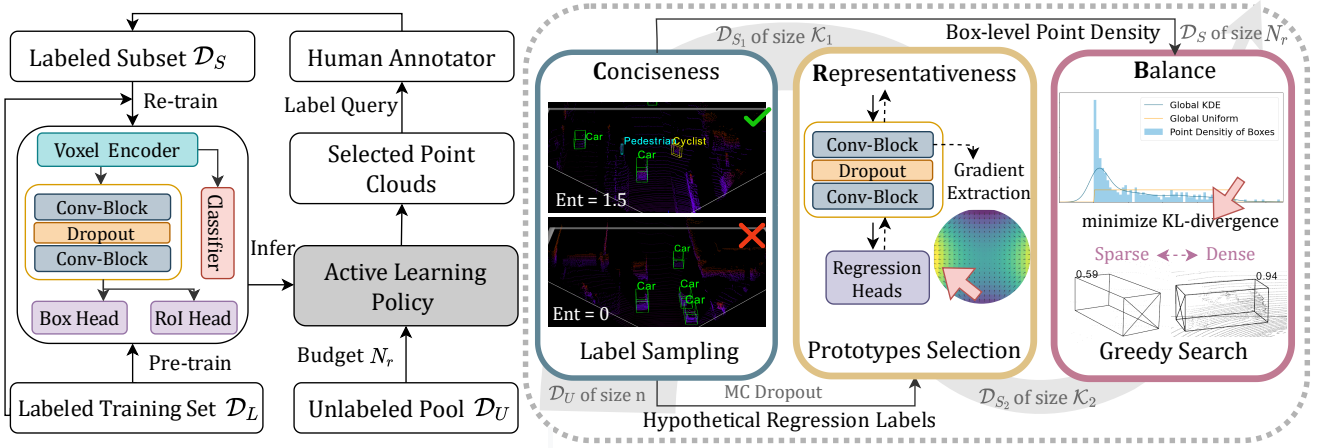


Fig. 2: An illustrative flowchart of the proposed CRB framework for the CWAL-3D task. Motivated by optimizing the generalization risk, the derived strategy hierarchically selects point clouds that have non-redundant bounding box labels, latent gradients and geometric characteristics to mitigate the gap with the test set and minimize annotation costs.

criteria (illustrated in Figure. 2): we first pick \mathcal{K}_1 candidates by concise label sampling (**Stage 1**), from which we select \mathcal{K}_2 representative prototypes (**Stage 2**), with $\mathcal{K}_1, \mathcal{K}_2 \ll n$. Finally, we leverage greedy search (**Stage 3**) to find the N_r prototypes that match with the prior marginal distribution of test data. The hierarchical sampling scheme can save $\mathcal{O}((n - \mathcal{K}_1)T_2 + (n - \mathcal{K}_2)T_3)$ cost, with T_2 and T_3 indicating the runtime of criterion evaluation. The detailed algorithm is summarized in (Luo et al 2023b). In the following, we describe the details of the three stages.

3.3.1 Stage 1: Concise Label Sampling (Cls)

By using *label conciseness* as a sampling criterion, we aim to alleviate label redundancy and align the source label distribution with the target prior label distribution. Particularly, we find a subset $\mathcal{D}_{S_1}^*$ of size \mathcal{K}_1 that minimizes Kullback-Leibler (KL) divergence between the probability distribution P_{Y_S} and the uniform distribution P_{Y_T} . To this end, we formulate the KL-divergence with Shannon entropy $H(\cdot)$ and define an optimization problem of maximizing the entropy of the label distributions:

$$D_{KL}(P_{\hat{Y}_{S_1}} \| P_{Y_T}) = -H(\hat{Y}_{S_1}) + \log |\hat{Y}_{S_1}|, \quad (2)$$

$$\begin{aligned} \mathcal{D}_{S_1}^* &= \arg \min_{\mathcal{D}_{S_1} \subset \mathcal{D}_U} D_{KL}(P_{\hat{Y}_{S_1}} \| P_{Y_T}) \\ &= \arg \max_{\mathcal{D}_{S_1} \subset \mathcal{D}_U} H(\hat{Y}_{S_1}), \end{aligned} \quad (3)$$

where $\log |\hat{Y}_{S_1}| = \log \mathcal{K}_1$ indicates the number of values Y_{S_1} can take on, which is a constant. Note that P_{Y_T} is a uniform distribution, and we removed the constant values from the formulations. We pass all point clouds $\{(\mathcal{P})_j\}_{j \in [n]}$ from the unlabeled pool to the detector and extract the predictive labels $\{\hat{y}_i\}_{i=1}^{N_B}$ for N_B bounding boxes, with $\hat{y}_i = \arg \max_{y \in [C]} f(x_i; \mathbf{w}_f)$. The label entropy of the j -th point cloud $H(\hat{Y}_{j,S})$ can be calculated as,

$$\begin{aligned} H(\hat{Y}_{j,S}) &= - \sum_{c=1}^C \mathbf{p}_{j,c} \log \mathbf{p}_{j,c}, \\ \mathbf{p}_{j,c} &= \frac{\sum_{i=1}^{N_B} \mathbb{1}(\hat{y}_i = c)}{N_B}, \end{aligned} \quad (4)$$

where $\mathbb{1}(\cdot)$ is the conditional enumerator. Based on the calculated entropy scores, we filter out the top- \mathcal{K}_1 candidates and validate them through the **Stage 2** representative prototype selection.

3.3.2 Stage 2: Representative Prototype Selection (RPS)

In this stage, we aim to identify whether the subsets cover the *unique* knowledge encoded only in \mathcal{D}_U and not in \mathcal{D}_L by measuring the *feature representativeness* with gradient vectors of point clouds. Motivated by this, we find the representative prototypes on the gradient space \mathcal{G} to form the subset \mathcal{D}_{S_2} , where magnitude and orientation represent the uncertainty and diversity of the new knowledge. For a classification problem, gradients can be retrieved by feeding the hypothetical label

$\hat{y} = \arg \max_{y \in [C]} \mathbf{p}(y|x)$ to the networks. However, the gradient extraction for regression problem is not explored yet in the literature, due to the fact that the hypothetical labels for regression heads cannot be directly obtained. To mitigate this, we propose to enable Monte Carlo dropout (Mc-dropout) at the **Stage 1**, and get the averaging predictions \bar{B} of M stochastic forward passes through the model as the hypothetical labels for regression loss:

$$\bar{B} \approx \frac{1}{M} \sum_{i=1}^M g(\mathbf{x}; \mathbf{w}_d, \mathbf{w}_g), \mathbf{w}_d \sim \text{Bernoulli}(1-p), \quad (5)$$

$$G_{S_2} = \{\nabla_{\Theta} \ell^{reg}(g(\mathbf{x}), \bar{B}; \mathbf{w}_g), \mathbf{x} \sim \mathcal{D}_{S_2}\}, \quad (6)$$

with p indicating the dropout rate, \mathbf{w}_d the random variable of the dropout layer, and Θ the parameters of the convolutional layer of the shared block. The gradient maps $G_{S_2} \in \mathcal{G}$ can be extracted from shared layers and calculated by the chain rule. Since the gradients for test samples are not observable, we make an assumption that its prior distribution follows a Gaussian distribution, which allows us to rewrite the optimization function as,

$$\begin{aligned} \mathcal{D}_{S_2}^* &= \arg \min_{\mathcal{D}_{S_2} \subset \mathcal{D}_{S_1}} D_{KL}(P_{X_{S_2}} \parallel P_{X_T}) \\ &\approx \arg \min_{\mathcal{D}_{S_2} \subset \mathcal{D}_{S_1}} D_{KL}(P_{G_{S_2}} \parallel P_{G_T}) \\ &= \arg \min_{\mathcal{D}_{S_2} \subset \mathcal{D}_{S_1}} \log \frac{\sigma_T}{\sigma_{S_2}} + \frac{\sigma_{S_2}^2 + (\mu_{S_2} - \mu_T)^2}{2\delta_T^2} - \frac{1}{2} \\ &\approx \mathcal{K}_2\text{-medoids}(G_{S_1}), \end{aligned} \quad (7)$$

with μ_{S_2} , σ_{S_2} (μ_T , and σ_T) being the mean and a standard deviation of the univariate Gaussian distribution of the selected set (test set), respectively. Based on Eq. 7, the task of finding a representative set can be viewed as picking \mathcal{K}_2 prototypes (*i.e.*, \mathcal{K}_2 -medoids) from the clustered data, so that the centroids (mean value) of the selected subset and the test set can be naturally matched. The variance σ_{S_2} and σ_T , basically, the distance of each point to its prototypes will be minimized simultaneously. We test different approaches for selecting prototypes in (Luo et al 2023b).

3.3.3 Stage 3: Greedy Point Density Balancing

The third criterion adopted is *geometric balance*, which targets at aligning the distribution of selected prototypes with the marginal distribution of testing point clouds. As point clouds typically consist of thousands (if not millions) of points, it is computationally expensive to directly align the meta features (*e.g.*, coordinates)

of points. Furthermore, in representation learning for point clouds, the common practice of using voxel-based architecture typically relies on quantized representations of point clouds and loses the object details due to the limited perception range of voxels. Therefore, we utilize the point density $\phi(\cdot, \cdot)$ within each bounding box to preserve the geometric characteristics of an object in 3D point clouds. By aligning the geometric characteristic of the selected set and unlabeled pool, the fine-tuned detector is expected to predict more accurate localization and size of bounding boxes and recognize both close (*i.e.*, dense) and distant (*i.e.*, sparse) objects at the test time. The probability density function (PDF) of the point density is not given and has to be estimated from the bounding box predictions. To this end, we adopt Kernel Density Estimation (KDE) using a finite set of samples from each class which can be computed as:

$$\mathbf{p}(\phi(\mathcal{P}, \hat{\mathcal{B}})) = \frac{1}{N_B h} \sum_{j=1}^{N_B} \mathcal{Ker}\left(\frac{\phi(\mathcal{P}, \hat{\mathcal{B}}) - \phi(\mathcal{P}, \hat{\mathcal{B}}_j)}{h}\right), \quad (8)$$

with $h > 0$ being the pre-defined bandwidth that can determine the smoothing of the resulting density function. We use Gaussian kernel for the kernel function $\mathcal{Ker}(\cdot)$. With the PDF defined, the optimization problem of selecting the final candidate sets \mathcal{D}_S of size N_r for the label query is:

$$\mathcal{D}_S^* = \arg \min_{\mathcal{D}_S \subset \mathcal{D}_{S_2}} D_{KL}(\phi(\mathcal{P}_S, \hat{\mathcal{B}}_S) \parallel \phi(\mathcal{P}_T, \mathcal{B}_T)), \quad (9)$$

where $\phi(\cdot, \cdot)$ measures the point density for each bounding box. We use greedy search to find the optimal combinations from the subset \mathcal{D}_{S_2} that can minimize the KL distance to the uniform distribution $\mathbf{p}(\phi(\mathcal{P}_T, \mathcal{B}_T)) \sim \text{uniform}(\alpha_{lo}, \alpha_{hi})$. The upper bound α_{hi} and lower bound α_{lo} of the uniform distribution are set to the 95% density interval, *i.e.*, $\mathbf{p}(\alpha_{lo} < \phi(\mathcal{P}, \hat{\mathcal{B}}_j) < \alpha_{hi}) = 95\%$ for every predicted bounding box j . Notably, the density of each bounding box is recorded during the **Stage 1**, which will not cause any computation overhead. The analysis of time complexity against other active learning methods is presented in (Luo et al 2023b).

Nevertheless, the CRB approach is primarily grounded in the assumption that the pre-training dataset and the unlabeled pool share the same set of classes, adhering to a closed-world active learning paradigm. The question arises: *How can CRB be extended to open-world scenarios, where unknown classes exist in the unlabeled data stream?*

3.4 Problem Definition of OWAL-3D

Definition 4 (OWAL-3D) Different from CWAL-3D where \mathcal{D}_L and \mathcal{D}_U shared the same class set $\mathcal{Y} = \{1, \dots, C\}$, the Open World Active Learning for 3D Object Detection (OWAL-3D) pipeline assumes that the unlabeled pool sourced from the open world \mathcal{D}_O , contains unknown/novel classes $\{C+1, \dots, C+U\}$ which do not exist in \mathcal{D}_L . The objective of OWAL-3D is to design a active selection strategy that selects a subset of raw data $\{\mathcal{P}_j\}_{j \in [N_r]}$ from \mathcal{D}_O and queries the labels of 3D bounding boxes from an oracle $\Omega : \mathcal{P} \rightarrow \mathcal{B} \times \mathcal{Y}_O$ to construct $\mathcal{D}_S = \{(\mathcal{P}, \mathcal{B}, Y)_j\}_{j \in [N_r]}$, where $Y \in \mathcal{Y}_O = \{1, \dots, C, C+1, \dots, C+U\}$. The 3D detection model is pre-trained on \mathcal{D}_L with shared class set $\mathcal{Y} = \{1, \dots, C\}$ for active selection, and then retrained on $\mathcal{D}_S \cup \mathcal{D}_L$ with newly annotated novel classes \mathcal{Y}_O until the selected samples reach the final budget B .

4 Our Approach: Open-CRB

4.1 OWAL-3D: Motivation

We elucidated the core research questions of OWAL-3D in the introduction section: (1) effectively discern point clouds that are likely to encompass objects of unknown categories, (2) avoid the redundant selection of bounding boxes for both known and unknown objects to save annotation costs. To address these dual challenges, we extend the strategy of Concise Label (CL) sampling, initially designed to compute label entropy solely for known classes, to a more comprehensive selection criterion termed **Open Conciseness Label (OCL) sampling**. OCL is expected to explore *novel* categories while maintaining the label conciseness of known classes within the dataset. Adapting CL to novel class discovery is *non-trivial*: The detection models are purely trained on a limited known class set and are devoid of any knowledge concerning these unknown labels. Without predicting unknown labels, it is *infeasible* to compute the unknown-aware label entropy using Equ. (4) for each point cloud. To address this issue, observation of good capability of uncertainty-based methods motivates us to employ the confidence estimation for unknown classes (refer to empirical results: Figure 5 and analysis in Section 5.5). These findings align with the realm of uncertainty estimation studies (Malinin and Gales 2018; Van Amersfoort et al 2020; Zohar et al 2023) for unknown/out-of-distribution exploration. When tested in the open world, the detection model tends to assign less prediction confidence for

those unknown/out-of-distribution instances in comparison to previously known instances.

4.2 Open Concise Label (OCL) Sampling

To estimate unknown labels, we firstly replace the hard label predictions $\hat{y}_i = \arg \max_{y \in [C]} f(x_i; \mathbf{w}_f)$ in concise label sampling (CLS) by the soft ones $\tilde{y}_i = \max \circ f(x_i; \mathbf{w}_f)$. The soft label entropy of each point cloud $\tilde{H}(\hat{Y}_{j,S})$ can be calculated as:

$$\mathbf{p}_{j,c} = \frac{\sum_{i=1}^{N_B} \mathbb{1}(\hat{y}_i = c) \times \tilde{y}_i}{N_B}, \text{ for } c \in [1, C]. \quad (10)$$

Next, we introduce an additional class $C+1$ as unknown and estimate its soft label based on model uncertainty on all other known classes as:

$$\mathbf{p}_{j,C+1} = \frac{\sum_{i=1}^{N_B} (1 - \tilde{y}_i)}{N_B}. \quad (11)$$

After combing Eq. (10) and Eq. (11), the final OCL score can be measured as the unknown-aware soft label entropy for each point cloud:

$$\tilde{H}(\hat{Y}_{j,S}) = - \sum_{c=1}^{C+1} \mathbf{p}_{i,c} \log \mathbf{p}_{i,c}. \quad (12)$$

Remark 3 To discuss the properties of the derived OCL criterion, we give a simple example as below. Given that 3D object detector was pre-trained on **two** known classes denoted as 1 and 2, there exists a new class in the unlabeled pool. When testing on an arbitrary point cloud j sourced from the open world, we have n_1 and n_2 box predictions of class 1 and 2, respectively. Note that $n_1 + n_2 = N_B$. The average prediction confidence for classes 1 and 2 are $\bar{p}_1 = \frac{\mathbf{p}_{j,1}}{n_1} N_B$ and $\bar{p}_2 = \frac{\mathbf{p}_{j,2}}{n_2} N_B$. Referring to Eq. (11), the unknown label components can be simplified:

$$\mathbf{p}_{j,C+1} N_B = n_1(1 - \bar{p}_1) + n_2(1 - \bar{p}_2), \quad (13)$$

$$N_B - \sum_i \tilde{y}_i = (n_1 + n_2) - \sum_i \tilde{y}_i$$

The most desired case is when soft label entropy $\tilde{H}(\hat{Y}_{j,S})$ is maximized, we have,

$$n_1 \bar{p}_1 = n_2 \bar{p}_2 = n_1(1 - \bar{p}_1) + n_2(1 - \bar{p}_2). \quad (14)$$

It can be interpreted as achieving maximum diversity in selecting both known and unknown classes equally. This equation leads to the following two relationships:

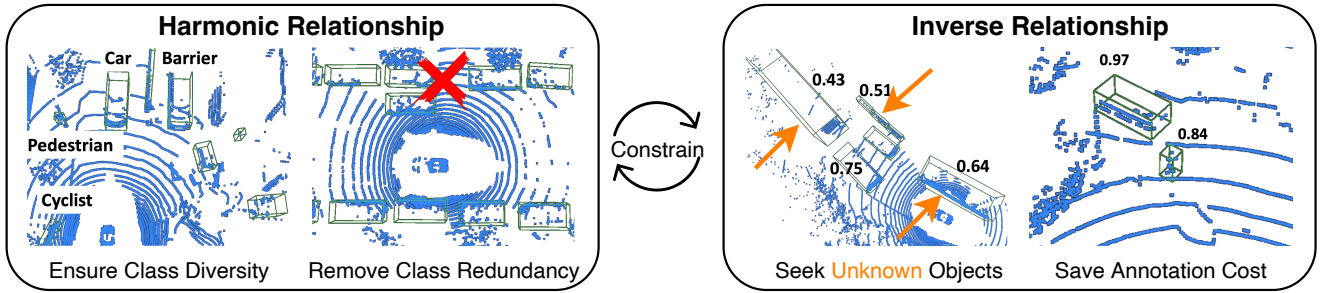


Fig. 3: Illustration of the proposed flowchart of Open Label Conciseness (OLC) for active selection from unlabeled open world pool. The proposed selection criteria (Eq. (12)) holds two relationships (Remark 3). The first involves a harmonic balance among confidences associated with different predicted classes, ensuring diversity and avoiding redundant categories within the selected point clouds. The second relationship is inversely proportional, linking the number of bounding boxes with confidence levels. This relationship aims to either 1) explore unknown objects from a large number of low-confidence predictions, or 2) reduce the number of bounding boxes if the existence of unknown objects is unlikely. These dual relationships constrain each other to select point clouds with concise labels and potentially unknown labels.

Harmonic Relationship: By substituting n_1 and n_2 in the Eq. (14), we can obtain the harmonic relationship between the averaged known confidences \bar{p}_1 and \bar{p}_2 :

$$\frac{2\bar{p}_1\bar{p}_2}{\bar{p}_1 + \bar{p}_2} = const. \quad (15)$$

The constant equals to $2/3$ when $C=2$. This relationship is a harmonic mean of the averaged confidence among the known classes. If a class is absent, this relationship will be difficult to maintain. Hence, this relation guarantees that the selected point cloud contains a diverse category distribution. As shown in the left two scenarios of Figure 3, the left example is preferred as it contains objects of multiple different categories, while the right one will lead to very low label entropy and not be selected by OLC.

Inverse Relationship: On the other side, when we substitute \bar{p}_1 or \bar{p}_2 in Eq. (14), we can derive the following constraints between the averaged confidence and the selected instance numbers:

$$\frac{n_2}{n_1} \propto \bar{p}_1, \quad \frac{n_1}{n_2} \propto \bar{p}_2. \quad (16)$$

This equation shows an inverse relationship between n_1 and \bar{p}_1 , and for n_2 and \bar{p}_2 vice versa. When n_2 is fixed and samples are of low confidence $\bar{p}_1 \downarrow$, this criterion will lead to picking more such instances ($n_1 \uparrow$). This selection rule can help identify more unknown instances, as illustrated in the third example of Figure 3. Conversely, A high averaged confidence $\bar{p}_1 \uparrow$ generally indicates a high likelihood of the point cloud containing a familiar known class, thus this equation will penalize $n_1 \downarrow$ to minimize the number of boxes, as depicted in the last case of Figure 3.

Therefore, the harmonic relationship compels the AL strategy to favor the point clouds with various categories, whereas the inverse relationship dynamically mines objects of novel categories or preserves annotations. These dual relationships constraint each other to ensure the selection of point clouds not only with a diverse and concise set of classes in limited numbers, but also with high likelihood to contain unknown categories.

5 Experiments

5.1 Datasets

KITTI (Geiger et al 2012) is one of the most representative datasets for point cloud based object detection. The dataset consists of 3,712 training samples (*i.e.*, point clouds) and 3,769 *val* samples. The dataset includes a total of 80,256 labeled objects with three commonly used classes for autonomous driving: cars, pedestrians, and cyclists. To fairly evaluate baselines and the proposed method on KITTI dataset (Geiger et al 2012), we follow the work of (Shi et al 2020): we utilize Average Precision (AP) for 3D and bird eye view (BEV) detection, and the task difficulty is categorized to Easy, Moderate, and Hard, with a rotated IoU threshold of 0.7 for cars and 0.5 for pedestrian and cyclists. The results evaluated on the validation split are calculated with 40 recall positions.

Waymo Open dataset (Sun et al 2020) is a challenging testbed for autonomous driving comprised of high resolution sensor data, containing 158,361 training samples and 40,077 testing samples. The point clouds contain 64 lanes of LiDAR corresponding to 180k points every

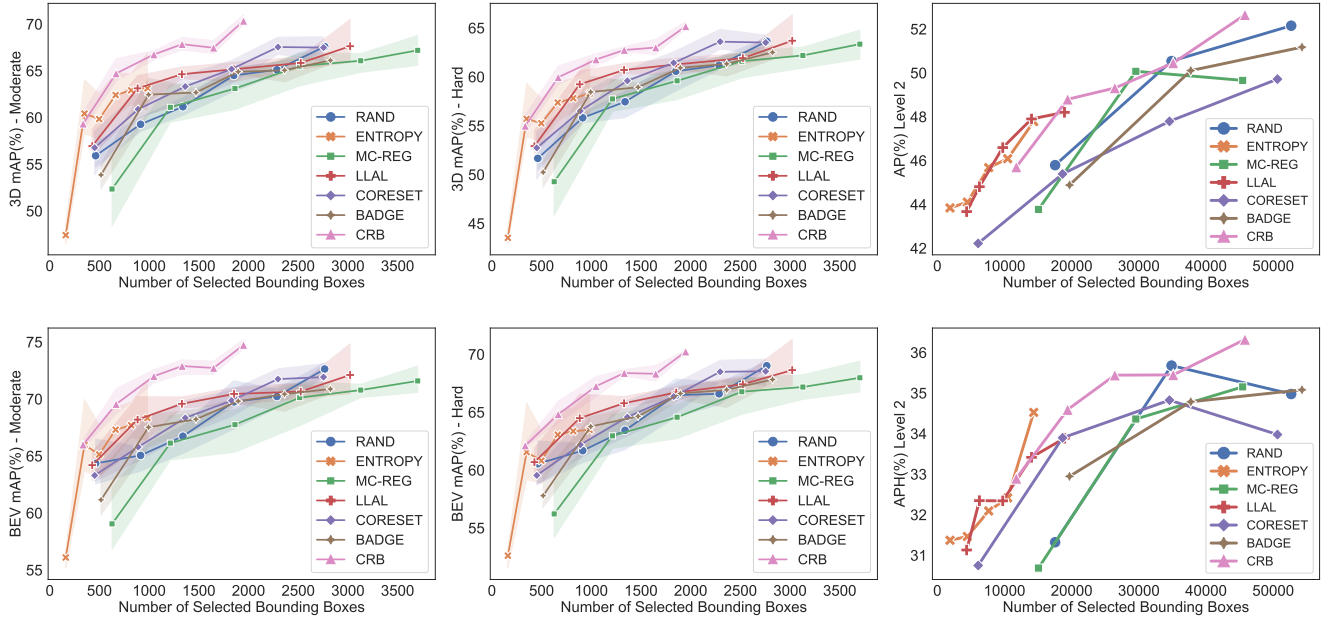


Fig. 4: CWAL-3D performance (3D and BEV mAP scores) comparisons of CRB and AL baselines on the KITTI and Waymo *val* split, with increasing annotation cost.

0.1s. To evaluate on Waymo dataset (Sun et al 2020), we adopt the officially published evaluation tool for performance comparisons, which utilizes AP and the average precision weighted by heading (APH). The respective IoU thresholds for vehicles, pedestrians, and cyclists are set to 0.7, 0.5, and 0.5. Regarding detection difficulty, the Waymo test set is further divided into two levels. Level 1 (and Level 2) indicates there are more than five inside points (at least one point) in the ground-truth objects. To alleviate computation overhead, we set the sampling interval to 10.

nuScenes dataset (Caesar et al 2020) comprises a total of 1000 driving sequences, which have been partitioned into three distinct subsets for the purposes of training, validation, and testing, encompassing 700, 150, and 150 sequences, respectively. These sequences, each possessing a temporal span of approximately 20 seconds, are characterized by a LiDAR data acquisition frequency of 20 frames per second (FPS). The nuScenes dataset (Caesar et al 2020) adopts two metrics: mean average precision (mAP) and nuScenes detection score (NDS). The former one is commonly employed but in nuScenes, they leverage the 2D center distance within the ground plane rather than IoU-based affinities. The latter is a weighted metric based on mAP and average error of translation, scale, orientation, velocity and attribute.

5.1.1 Evaluation Metric for OWAL-3D

To thoroughly assess the effectiveness of various methods within the OWAL-3D context, we establish three specific metrics tailored to open world active learning for 3D object detection. These metrics measure the methodology capacity to 1) explore unknown classes, 2) accurately recognize all classes, and 3) save the associated annotation costs.

Performance across unknown classes: mAP_{unk} . We average the AP score for all unknown categories:

$$mAP_{unk} = \frac{1}{U} \sum_{i=1}^U AP_i, i \in \{1, \dots, U\} \quad (17)$$

where AP_i indicates the AP score of $(C + i)$ -the class, calculated by KITTI or nuScenes official metric. A high score of mAP_{unk} signifies that the 3D detection model has gained sufficient knowledge of the novel class within the open world.

Balanced performance across all classes: mAP_H . We compute the harmonic mean between mAP_{unk} and the mean AP across known classes mAP_k as:

$$mAP_H = \frac{2}{1/mAP_{unk} + 1/mAP_k}, \quad (18)$$

$$mAP_k = \frac{1}{C} \sum_{j=1}^C AP_j, j \in \{1, \dots, C\}. \quad (19)$$

The harmonic mean was widely adopted in previous work (Scheirer et al 2013; Geng et al 2021; Luo et al

2023c) related to open-set task, which helps to prevent any bias towards either unknown classes or known classes, indicating balanced and unbiased results.

Annotation Cost. According to the preliminary study (Luo et al 2023b), we utilize the total number of labeled bounding boxes across all selected point clouds as the unit for realist annotation cost. The lower, the better.

5.2 Implementation Details

To ensure the reproducibility of the baselines and the proposed approach, the source code has been made publicly available, including comprehensive training and test configurations and is readily executable for accessibility and ease of use. For fair comparison, all methods are constructed from the Pv-rcnn (Shi et al 2020) and Second (Yan et al 2018) backbones. All experiments are conducted on a GPU cluster with three V100 GPUs. Training Pv-rcnn on the full set typically requires 20 GPU hours for KITTI and 120 GPU hours for Waymo. While training SECOND requires 10 GPU hours for KITTI and 80 GPU hours for nuScenes.

Parameter Settings. The batch sizes for training and evaluation are fixed to 8, 8 and 16 on KITTI, nuScenes and Waymo, respectively. The Adam optimizer is adopted with a learning rate initiated as 0.01, and scheduled by one cycle scheduler. The number of Mc-dropout stochastic passes is set to 5 for all methods. The \mathcal{K}_1 and \mathcal{K}_2 are empirically set to 300, 200 for KITTI, 2,000 and 1,500 for nuScenes and 2,000 and 1,200 for Waymo. The gradient maps used for Rps are extracted from the second convolutional layer in the shared block of the 3D detector. Three dropout layers are enabled during the Mc-dropout and the dropout rate is fixed to 0.3 for both datasets. The number of Mc-dropout stochastic passes are set to 5 for all methods.

CWAL-3D Protocols. As our work is the first comprehensive study on active learning for 3D detection task, the active training protocol for all AL baselines and the proposed method is empirically defined. For all experiments, we first randomly select m fully labeled point clouds from the training set as the initial \mathcal{D}_L . With the annotated data, the 3D detector is trained with E epochs, which is then freed to select N_r candidates from \mathcal{D}_U for label acquisition. We set the m and N_r to 2.5 3% point clouds (*i.e.*, $N_r = m = 100$ for KITTI, $N_r = m = 400$ for Waymo) to trade-off between reliable model training and high computational costs. The aforementioned training and selection steps will alternate for R rounds. Empirically, we set $E = 30$, $R = 6$ for KITTI, and fix $E = 40$, $R = 5$ for Waymo.

OWAL-3D Protocols. Based on the CWAL-3D protocols, we empirically adopt a similar setup for the

OWAL-3D. Specifically, We define $N_r = 200$, $m = 100$ for KITTI and $N_r = 3000$, $m = 1500$ for nuScenes. The aforementioned training and selection steps will alternate for R rounds. Empirically, we set $E = 40$, $R = 4$ for both KITTI and nuScenes. Regarding the known and unknown class separation we randomly select a subset of common object categories (*i.e.* car, motorcycle, bicycle, pedestrian, and truck) to serve as known classes in nuScenes dataset. The rest of classes (*i.e.* construction vehicle, bus, trailer, barrier, and traffic cone) are unknown. As for the KITTI dataset with only three classes, we set car and cyclist as known classes, and pedestrian as unknown.

5.3 Baselines

We introduce a large-scale, open-sourced benchmark ¹ for both CWAL-3D and OWAL-3D named, featuring meticulous evaluations, comprehensive analyses as well as 14 extensive cutting-edge baseline algorithms of AL, OW-OD and out-of-distribution (OOD):

Generic Active Learning Baselines:

- (1) **Rand**: is a basic sampling method that selects N_r samples at random for each selection round;
- (2) **Entropy** (Wang and Shang 2014): is an *uncertainty*-based active learning approach that targets the *classification* head of the detector, and selects the top N_r ranked samples based on the entropy of the sample’s predicted label;
- (3) **LLAL** (Yoo and Kweon 2019): is an *uncertainty*-based method that adopts an auxiliary network to predict an indicative loss and enables to select samples for which the model is likely to produce wrong predictions;
- (4) **Coreset** (Sener and Savarese 2018): is a *diversity*-based method performing the core-set selection that uses the greedy furthest-first search on both labeled and unlabeled embeddings at each round;
- (5) **Badge** (Ash et al 2020): is a *hybrid* approach that samples instances that are disparate and of high magnitude when presented in a hallucinated gradient space.
- (6) **Bait** (Ash et al 2021): selects batches of samples by optimizing a bound on the maximum likelihood estimators (MLE) error in terms of the Fisher information.

Applied AL Baselines for 2D and 3D Detection: for a fair comparison, we also compared three variants of the deep active learning method for 3D detection and adapted one 2D active detection method to our 3D detector.

¹ accessible at <https://github.com/Luoyadan/CRB-active-3Ddet>

Table 1: CWAL-3D performance (3D AP scores) comparisons with generic AL and applied AL for detection on KITTI *val* set with 1% queried bounding boxes.

Method	Car			Pedestrian			Cyclist			Average			
	Easy	Mod.	Hard	Easy	Mod.	Hard	Easy	Mod.	Hard	Easy	Mod.	Hard	
Generic	Coreset	87.77	77.73	72.95	47.27	41.97	38.19	81.73	59.72	55.64	72.26	59.81	55.59
	Badge	89.96	75.78	70.54	51.94	46.24	40.98	84.11	62.29	58.12	75.34	61.44	56.55
	LLAL	89.95	78.65	75.32	56.34	49.87	45.97	75.55	60.35	55.36	73.94	62.95	58.88
AL-Det	Mc-reg	88.85	76.21	73.47	35.82	31.81	29.79	73.98	55.23	51.85	66.21	54.41	51.70
	Mc-mi	86.28	75.58	71.56	41.05	37.50	33.83	86.26	60.22	56.04	71.19	57.77	53.81
	Consensus	90.14	78.01	74.28	56.43	49.50	44.80	78.46	55.77	53.73	75.01	61.09	57.60
	Lt/c	88.73	78.12	73.87	55.17	48.37	43.63	83.72	63.21	59.16	75.88	63.23	58.89
CRB	90.98	79.02	74.04	64.17	54.80	50.82	86.96	67.45	63.56	80.70	67.81	62.81	

Table 2: CWAL-3D performance (3D and BEV mAP scores) comparisons on the KITTI *val* split with one-stage 3D detector Second.

	3D Detection mAP			BEV Detection mAP		
	Easy	Moderate	Hard	Easy	Moderate	Hard
Rand	69.33 \pm 0.62	55.48 \pm 0.43	51.53 \pm 0.33	75.66 \pm 1.10	63.77 \pm 0.86	59.71 \pm 0.95
Coreset (Sener and Savarese 2018)	66.86 \pm 2.27	53.22 \pm 1.65	48.97 \pm 1.42	73.08 \pm 1.80	61.03 \pm 1.98	56.95 \pm 1.53
LLAL (Yoo and Kweon 2019)	69.19 \pm 3.43	55.38 \pm 3.63	50.85 \pm 3.24	76.52 \pm 2.24	63.25 \pm 3.11	59.07 \pm 2.80
Badge (Ash et al 2020)	69.92 \pm 2.90	55.60 \pm 2.72	51.23 \pm 2.58	76.07 \pm 2.70	63.39 \pm 2.52	59.47 \pm 2.49
Bait (Ash et al 2021)	69.45 \pm 3.53	55.61 \pm 2.94	51.25 \pm 2.42	76.04 \pm 1.75	63.49 \pm 2.14	53.40 \pm 2.00
CRB (Luo et al 2023b)	72.33 \pm 0.35	58.06 \pm 0.30	53.09 \pm 0.31	78.84 \pm 0.27	65.82 \pm 0.07	61.25 \pm 0.22

Table 3: Study of different proposed CWAL-3D selection criteria on the KITTI *val* split. 3D and BEV AP scores (%) are reported when 1,000 bounding boxes are annotated.

Cls	Rps	Gpdb	3D Detection mAP			BEV Detection mAP		
			Easy	Moderate	Hard	Easy	Moderate	Hard
-	-	-	70.70 \pm 1.60	58.27 \pm 1.04	54.69 \pm 1.30	75.37 \pm 1.65	64.54 \pm 1.69	61.36 \pm 1.61
✓	-	-	77.76 \pm 1.70	64.56 \pm 1.39	59.54 \pm 1.13	81.07 \pm 1.67	69.76 \pm 1.45	65.01 \pm 1.31
-	✓	-	74.93 \pm 3.11	61.65 \pm 1.95	57.70 \pm 1.52	78.85 \pm 2.31	67.07 \pm 1.36	63.47 \pm 1.21
-	-	✓	69.11 \pm 13.22	56.12 \pm 12.74	52.85 \pm 11.49	73.57 \pm 10.45	62.49 \pm 10.62	59.45 \pm 9.78
✓	✓	-	76.19 \pm 2.13	62.81 \pm 1.31	58.03 \pm 1.18	80.73 \pm 0.92	68.67 \pm 0.21	64.42 \pm 0.22
✓	-	✓	76.72 \pm 0.78	64.70 \pm 1.07	59.68 \pm 0.93	80.71 \pm 0.26	70.01 \pm 0.40	65.47 \pm 0.56
✓	✓	✓	79.03 \pm 1.39	65.86 \pm 1.21	61.06 \pm 1.43	82.60 \pm 1.34	70.74 \pm 0.57	66.41 \pm 1.22

(7) **Mc-mi** (Feng et al 2019) utilized Monte Carlo dropout associated with mutual information to determine the uncertainty of point clouds.

(8) **Mc-reg**: additionally, to verify the importance of the uncertainty in regression, we design an *uncertainty*-based baseline that determines the *regression* uncertainty via conducting M -round Mc-dropout stochastic passes at the test time. The variances of predictive results are then calculated, and the samples with the top- N_r greatest variance will be selected for label acquisition. We further adapted two applied AL methods for 2D detection to a 3D detection setting, where

(9) **Lt/c** (Kao et al 2018) measures the class-specific localization tightness, *i.e.*, the changes from the intermediate proposal to the final bounding box and

(10) **Consensus** (Schmidt et al 2020) calculates the variation ratio of minimum IoU value for each RoI-match of 3D boxes.

Applied AL Baselines for OW-OD and OOD: although existing OW-OD methods follows a different paradigms (*i.e.*, out-of-distribution detection (OOD) / open-set recognition plus continual learning), we can still implement unknown exploration modules to detect potential unknown objects in 3D scenes. Thus, the

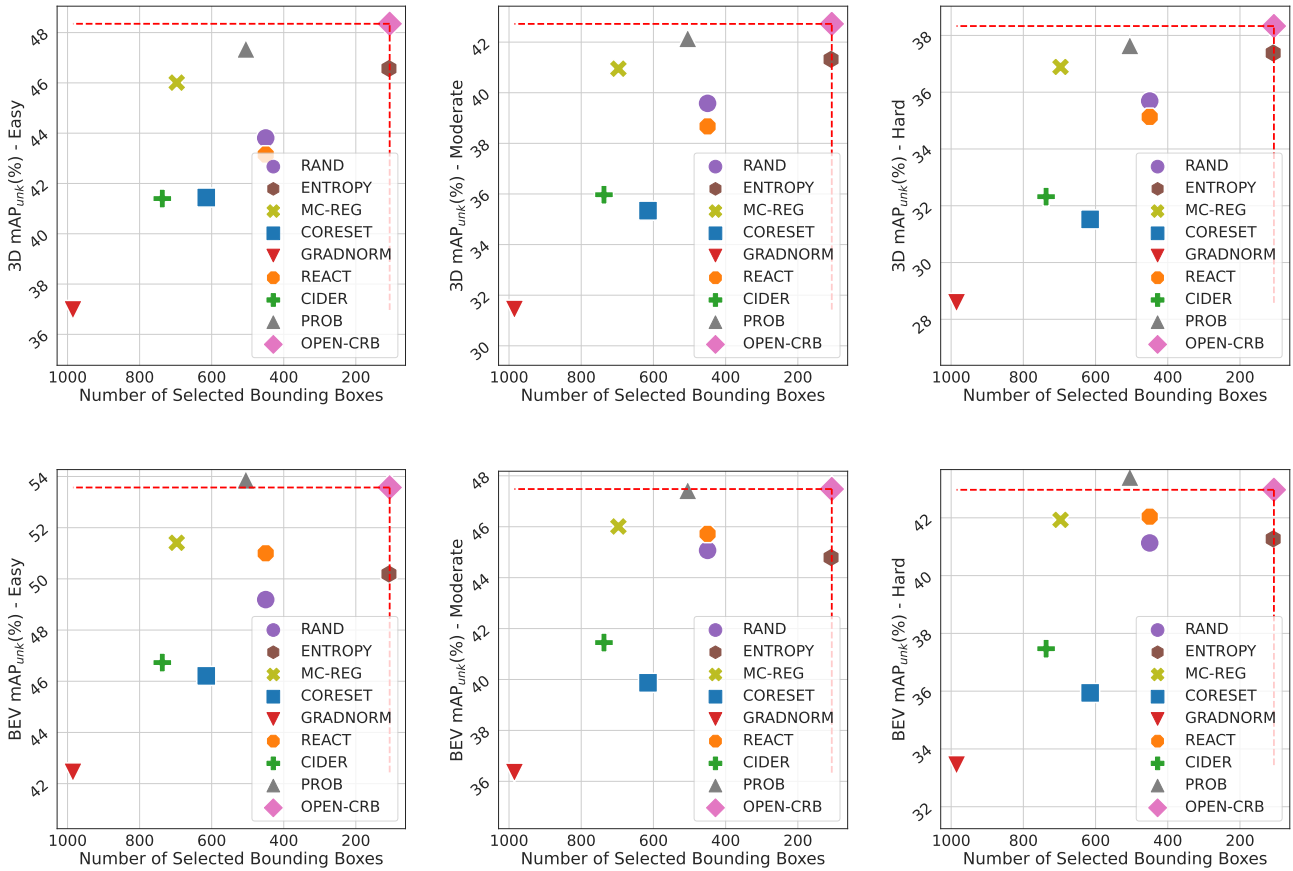


Fig. 5: OWAL-3D performance (3D and BEV mAP_{unk} scores) comparisons on unknown classes of CRB and baselines on the KITTI dataset.

AL strategy becomes selecting point clouds with higher probability to contain unknown objects.

(11) **PROB** (Zohar et al 2023) integrates probabilistic models into the object detector to facilitate objectiveness estimation within the embedded feature space. Then, point clouds containing higher averaged estimated objectiveness are selected.

(12) **GradNorm** (Huang et al 2021) splits in-distribution (ID) and OOD data based on the vector norm of gradients, backpropagated from the discrepancy between the softmax output and a uniform probability distribution.

(13) **ReAct** (Liu et al 2020) separates the ID and OOD data after rectifying the activations at an upper limit, based on the observation that OOD data have larger variations in activations.

(14) **Cider** (Ming et al 2023) formalizes the latent representations as vMF distributions, then calculate distances in hyperspherical embeddings, from data point to the class prototypes.

5.4 Main Results for CWAL-3D

We conducted comprehensive experiments on the KITTI and Waymo datasets to demonstrate the effectiveness of the proposed CRB approach for the CWAL-3D task. The \mathcal{K}_1 and \mathcal{K}_2 are empirically set to 300 and 200 for KITTI and 2,000 and 1,200 for Waymo. Under a fixed budget of point clouds, the performance of 3D and BEV detection achieved by different AL policies are reported in Figure 4, with standard deviation of three trials shown in shaded regions. We can clearly observe that CRB consistently outperforms all state-of-the-art AL methods by a noticeable margin, irrespective of the number of annotated bounding boxes and difficulty settings. It is worth noting that, on the KITTI dataset, the annotation time for the proposed CRB is 3 times faster than Rand, while achieving a comparable performance. Moreover, AL baselines for regression and classification tasks (e.g., LLAL) or for regression only tasks (e.g., Mc-reg) generally obtain higher scores yet leading to higher

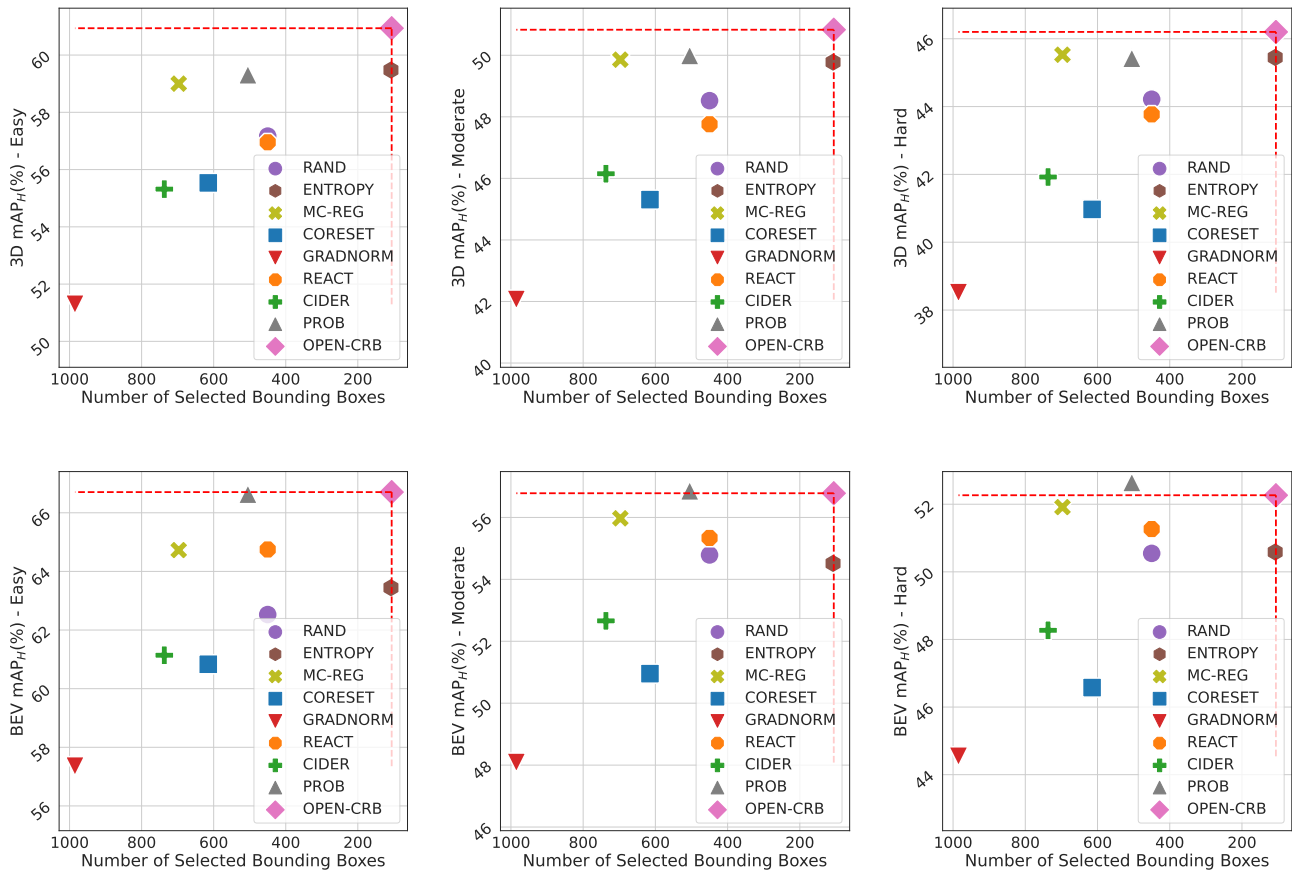


Fig. 6: OWAL-3D performance (mAP_H : 3D and BEV harmonic mean of known mAP and unknown mAP) comparisons on all the classes of CRB and baselines on the KITTI dataset.

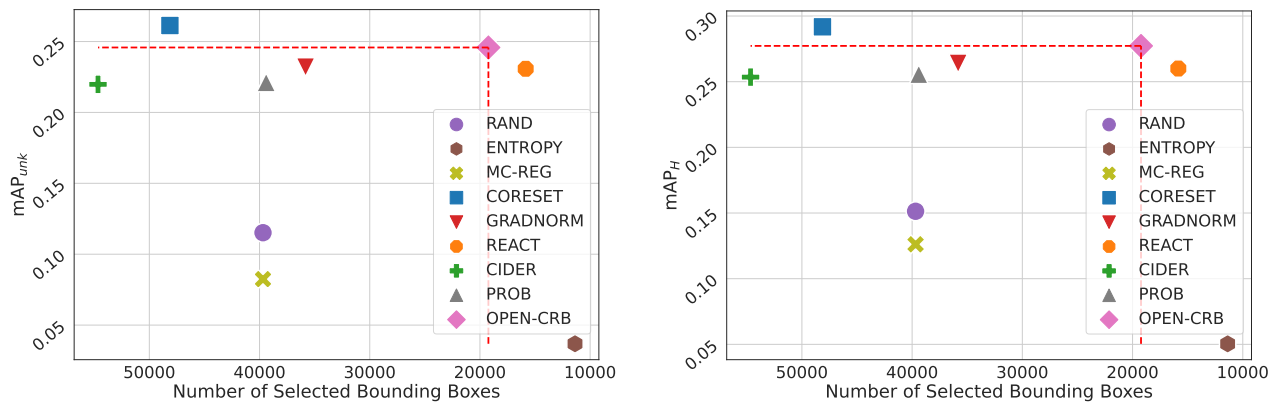


Fig. 7: OWAL-3D performance (left: mAP_{unk} , right: mAP_H) comparisons of CRB and baselines on the nuScenes dataset.

labeling costs than the classification-oriented methods (e.g., Entropy).

Table 1 reports the major experimental results of the state-of-the-art generic AL methods and applied AL approaches for 2D and 3D detection on the KITTI

dataset. It is observed that LLAL and Lt/c achieve competitive results, as the acquisition criteria adopted jointly consider the classification and regression task. Our proposed CRB improves the 3D mAP scores by 6.7% which validates the effectiveness of minimizing the generalization risk. More qualitative analysis can be found in (Luo et al 2023b).

Impact of Detector Architecture. We validate the sensitivity of performance to choices of one-stage and two-stage detectors. Table 2 reports the results with the Second detection backbone on the KITTI dataset. With only 3% queried 3D bounding boxes, it is observed that the proposed CRB approach consistently outperforms the SOTA generic active learning approaches across a range of detection difficulties, improving 4.7% and 2.8% on 3D mAP and BEV mAP scores.

Study of Active Selection Criteria. Table 3 reports the performance comparisons of six variants of the proposed CRB method and the basic random selection baseline (1-st row) on the KITTI dataset. We report the 3D and BEV mAP metrics at all difficulty levels with 1,000 bounding boxes annotated. We observe that only applying Gpdb (4-th row) produces 12.5% lower scores and greater variance than the full model (the last row). However, with Cls (6-th row), the performance increases by approximately 10% with the minimum variance. This phenomenon evidences the importance of optimizing the discrepancy for both classification and regression tasks. It’s further shown that removing any selection criteria from the proposed CRB triggers a drop on mAP scores, confirming the importance of each in a sample-efficient AL strategy.

5.5 Main Results for OWAL-3D

We performed extensive experiments on both the KITTI and nuScenes datasets to validate the efficacy of the proposed Open-CRB, utilizing SECOND as the backbone detector. We illustrate the relationship between annotation cost and the corresponding performance improvement through scatter plots, as depicted in Figure 5, Figure 6 and Figure 7.

Results on Unknown Classes. It is worth noting that the proposed Open-CRB suggested significantly surpasses other baseline techniques in enhancing the capability to recognize unknown classes after the first selection is found. For instance, the upper three plots in Figure 5 feature a horizontal dashed line, representing the best 3D mAP_{unk} achieved by Open-CRB for recognizing unknown classes. The most inspiring finding is that the group of uncertainty-based baselines (*e.g.*, Entropy, PROB and MC-Reg) achieve better mAP_{unk} than discrepancy-based methods (*e.g.*, Coreset and Cider).

This finding validates the effectiveness of uncertainty for learning unknown class and thus become the basis of our method. Turning to the nuScenes dataset, the left plot in Figure 6 demonstrates that Open-CRB secures the second-highest mAP_{unk} . Although Coreset achieves a slightly superior result, **it comes at the expense of 2.5 times the annotation cost when compared to Open-CRB.** Moreover, in the context of nuScenes, discrepancy-based methods (*e.g.*, Coreset and Cider) produce similar results to those of uncertainty-based baselines, however, at the expense of selecting a significantly higher number of bounding boxes. Overall, the impressive results demonstrated by the Open-CRB in unknown categories provide strong evidence that the proposed sampling technique is highly effective in selecting informative objects from novel categories within unlabeled point clouds. This approach significantly enhances the model’s ability to adapt to open world scenarios.

Results on All Classes. To evaluate the effectiveness of the proposed methods in recognizing both known and unknown classes, we adopt the widely used harmonic mean Average Precision (mAP_H) balanced between mAP_{unk} and mAP_k , and present the results in Figure 6 for KITTI and Figure 7 for nuScenes. A higher mAP_H indicates that the method not only performs better across all categories but also maintains a narrow gap between mAP_{unk} and mAP_k . In the case of KITTI, as depicted in Figure 6, the proposed Open-CRB consistently achieves the highest 3D mAP_H across all difficulty settings compared to other baselines, requiring the least annotation cost. The very recent state-of-the-art OW-OD method, PROB, achieves a slightly higher BEV mAP_H than Open-CRB (52.64% vs. 52.27%), but it costs significantly more annotated bounding boxes (505 vs. 106). Besides, PROB is not a post-hoc approach that requires additional computations at the pre-training phase, leading to more time consumption than Open-CRB. In the context of the more challenging label-rich dataset, nuScenes, Open-CRB continues to perform remarkably while incurring very limited labeling cost (19232 of labeled bounding boxes), securing a mAP_H that is second only to Coreset (48133 of labeled bounding boxes). These experimental results clearly demonstrate that our approach effectively enables the model to simultaneously learn both unknown and known classes, without bias.

Annotation Cost and Performance Balance. To assess the annotation cost across various approaches, we present the total count of labeled bounding boxes (encompassing both known and unknown classes) on the x-axis. It is clear that our approach stands out by significantly reducing the total number of annotations

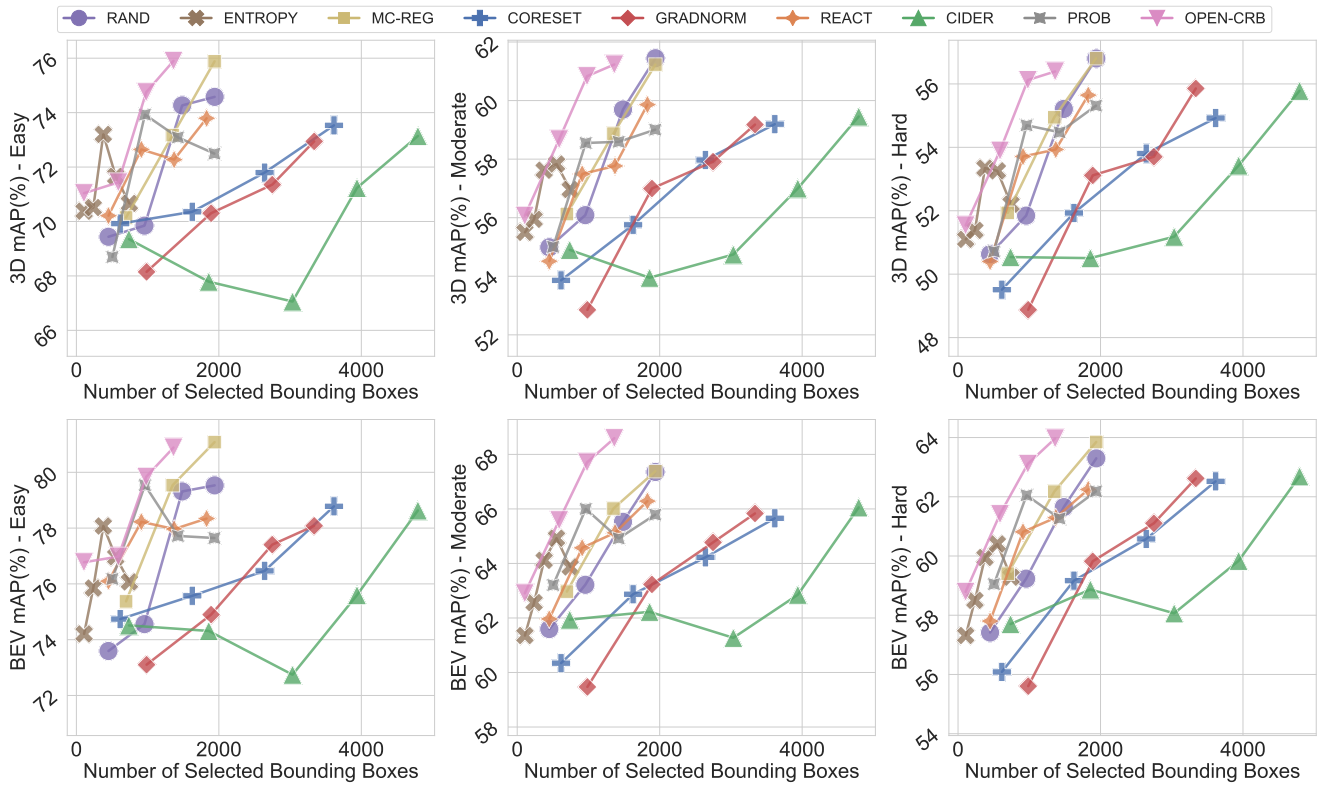


Fig. 8: OWAL-3D performance (3D and BEV mAP scores) comparisons of Open-CRB and AL baselines on the KITTI dataset, with increasing annotation cost.

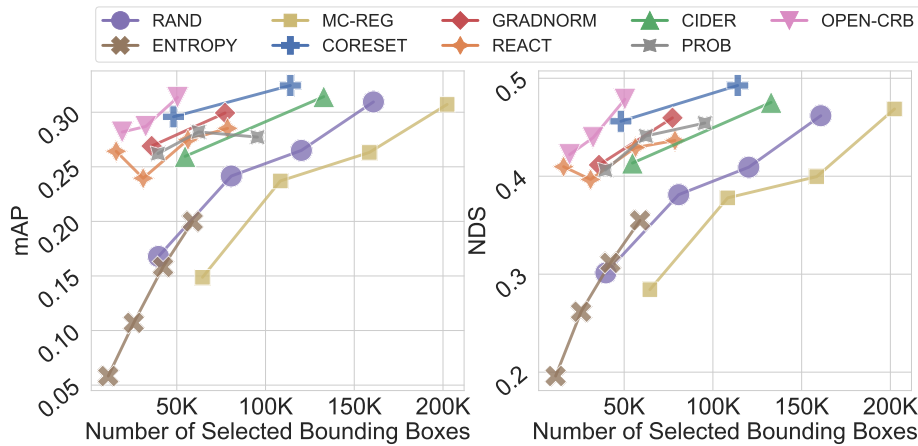


Fig. 9: OWAL-3D performance (mAP and NDS scores) comparisons of Open-CRB and AL baselines on the nuScenes dataset, with increasing annotation costs.

required (106 from KITTI and 8734 from nuScenes) compared to the majority of baseline methods, all while preserving the outstanding mAP_{unk} and mAP_H score. This holds especially true for KITTI, as evident from the scatter plots in Figure 6, our approach successfully reaches the **skyline point**, representing the optimum in both the dimension of performance and the dimension of annotation costs.

Results with Increasing Annotations. Additionally, we illustrate the performance trends in Figure 8 and Figure 9 for KITTI and nuScenes, respectively, depicting how performance evolves as the labeling costs increase during multi-round active selections and model training. We can clearly observe that Open-CRB consistently surpasses all state-of-the-art methods by a significant margin, regardless of the quantity of annotated

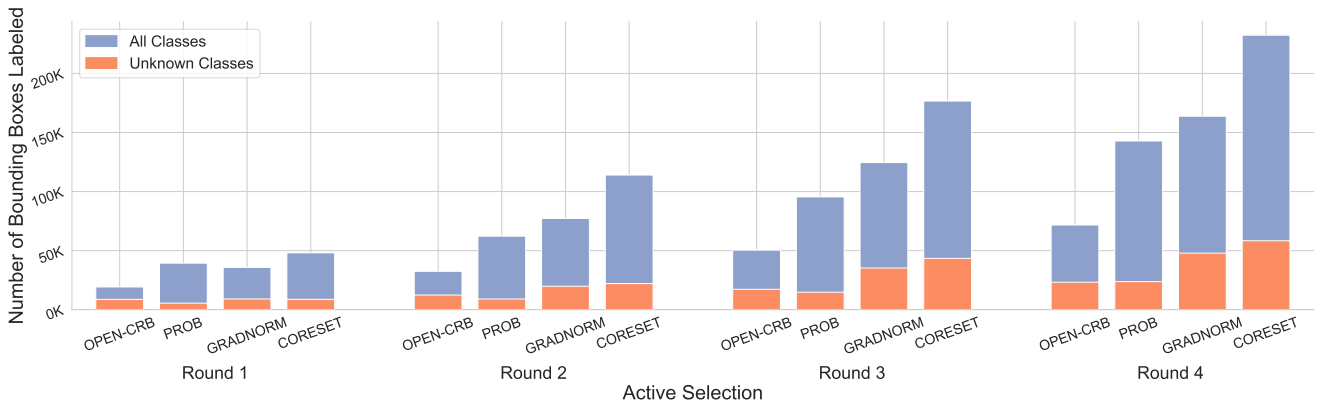


Fig. 10: The accumulation of the number of selected bounding boxes from nuScenes dataset, with active learning selection rounds increase, under the OWAL-3D setting.

bounding boxes, difficulty settings in KITTI or the evaluation metric used in nuScenes. It is remarkable that, on the nuScenes dataset, the annotation time for the proposed Open-CRB is three times quicker than Rand (approximately 50,000 annotations versus approximately 160,000 at round 3), while achieving comparable performance.

Analysis on Selected Labels. The experimental analysis above demonstrates the effectiveness of our proposed method in enhancing model performance. This success has sparked our curiosity about the specific source of performance improvement, in other words, the types of point clouds the model trains on to achieve these outstanding results. To investigate this, we delved into the composition of known and unknown labels within selected boxes using different methods, illustrated in Figure 10. We tracked the accumulated count of known and unknown boxes in the nuScenes dataset as the active selection round increases. Note that, while unseen classes were labeled after round 1, we continued to track them in subsequent active rounds. It is clear from the initial round, our method selected the fewest total boxes while the highest proportion of unknown instances: 45.41% of which belonged to unknown classes. In contrast, other methods not only incur higher costs but also fail to mine point clouds containing novel class objects. Specifically, for PROB, GradNorm, and Core-set, the percentages of selected unknown classes objects in the first round were 14.01%, 25.42%, and 18.25%, respectively. This highlights our approach as a targeted solution to the core challenge of OWAL-3D task: how to acquire point clouds housing potential novel class objects while minimizing annotation costs.

In the following active rounds, even though unknown instances are manually assigned with ground truth labels, they are transited into long-tail classes. This hap-

pens because, firstly, the model learned insufficient knowledge of these newly annotated classes for only one round, and secondly, these novel classes themselves are rare, such as construction vehicles and trailers. Therefore, our proposed approach, Open-CRB, based on the same principle of detecting novel classes, can effectively detect objects of long-tail classes, enhancing model performance by ensuring balanced learning across both known and unknown classes. In subsequent rounds, as illustrated in Figure 10, Open-CRB consistently maintains a high percentage of boxes belonging to these newly introduced classes. By the final round, the percentages of boxes for new arrival classes are 32.46%, 16.65%, 29.24%, and 25.11% for each method, respectively. These findings for composition (unknown/known) of acquired labels, serve as direct evidence that the proposed method achieves its intended objectives, as depicted in Figure 3.

Qualitative Analysis. Previous quantitative analysis on label selection proved the validity of the proposed Open-CRB. Now, we switch to a qualitative analysis of the acquired point clouds to gain a more intuitive understanding of the advantages of our proposed OWAL-3D strategy. Figures 11 and 12 display point clouds randomly sampled by Rand and Open-CRB, respectively. Figure 11 illustrates that the random approach tends to select commonplace scenes, such as many vehicles parking along the road, commonly found in real-world scenarios. The lower part of Figure 11 particularly showcases a significant number of pedestrians, indicating a known label redundancy. Consequently, the model tends to focus on recognizing previously known classes (*e.g.*, vehicles and pedestrians) and struggles to acquire novel knowledge. In contrast, our method selects point clouds encompassing a wide range of categories including both known and unknown, as depicted

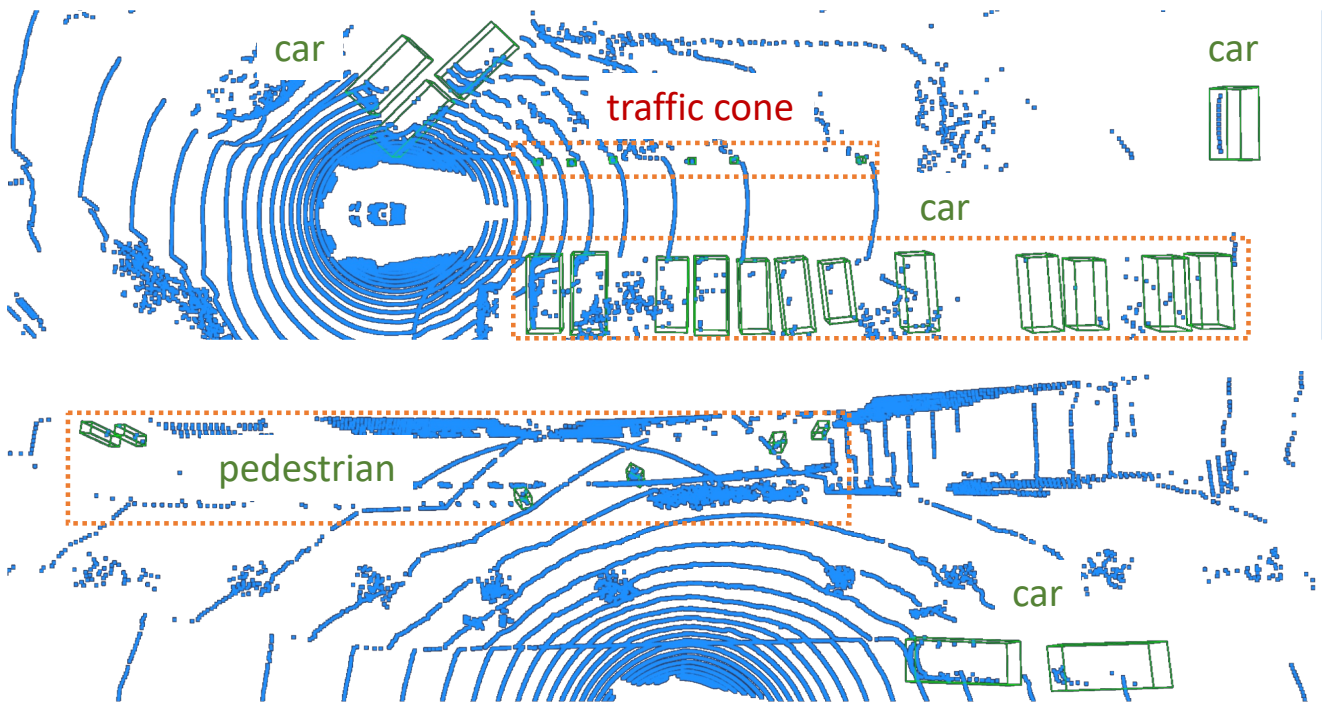


Fig. 11: Acquired point cloud by **Rand**, instances of novel category are highlighted in red.

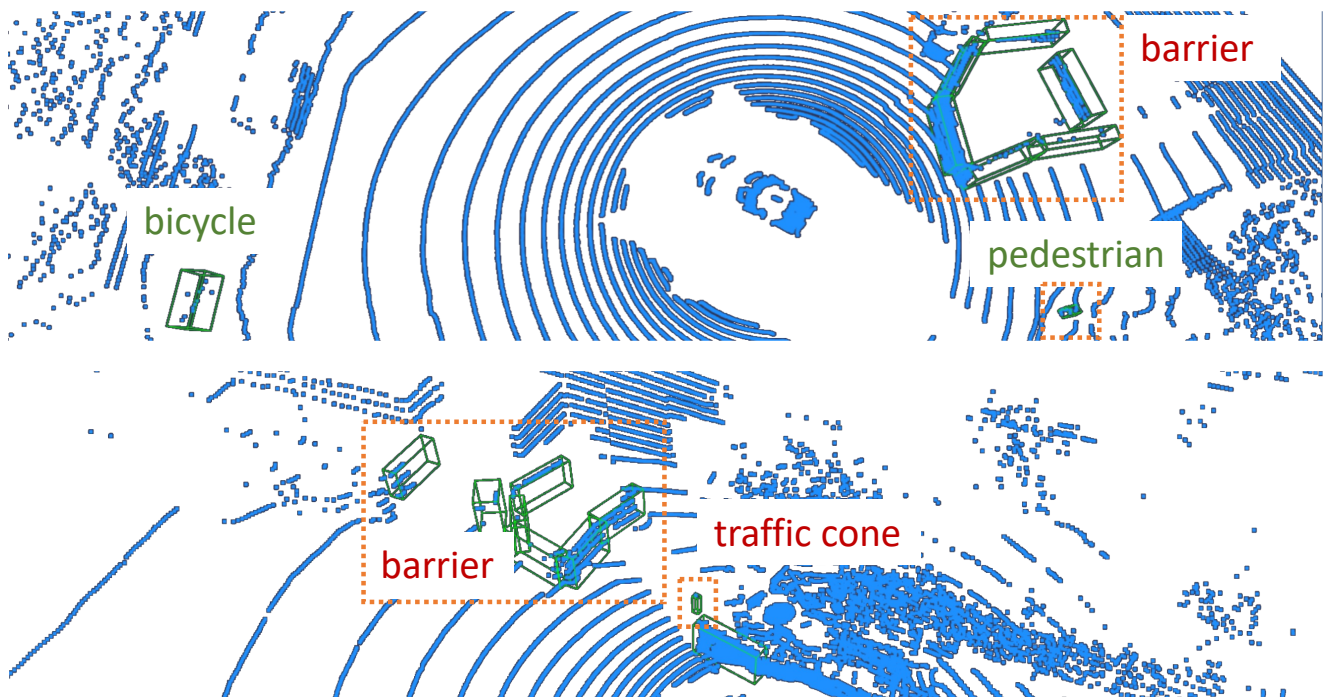


Fig. 12: Visualization of acquired point clouds by the proposed **Open-CRB** where instances of the novel category are highlighted in red.

in Figure 12. Additionally, Open-CRB excels in discovering relatively more novel objects, such as barriers, traffic cones, and buses highlighted in red. This demonstrates that the samples chosen by Open-CRB encom-

pass a broader and more concise range of both known and unknown classes, effectively enhancing the model performance in open world 3D scenes.

6 Discussion and Conclusion

In this paper, we investigate a novel and practical task: Open World Active Learning for 3D Object Detection (OWAL-3D), aiming to transfer contemporary 3D detection models to the open world environments containing novel/unknown object categories, with minimal annotation efforts. To explore OWAL-3D, we have developed an extensive open-source benchmark that incorporates 15 recent methods of active learning, out-of-distribution detection, and open world detection. We have also integrated three 3D detection datasets and two widely utilized backbone 3D detectors, catering to both OWAL-3D and closed world active learning scenarios. Based on the benchmark, we have proposed a simple yet highly efficient method called Open-CRB, tailored for OWAL-3D, as a remarkable point cloud acquisition strategy that boosts 3D object detection performance across both known and unknown object classes, requiring only minimal human annotations. However, Open-CRB faces two key limitations: (1) it estimates of the unknown label components rather than precisely localizes unknown instances, leading to an inability to find unknown objects during the test stage before the initial active round selection. (2) Open-CRB primarily addresses semantic shifts (i.e., category mismatches) between pre-trained and test data while overlooking covariate shifts within same classes and scene backgrounds. This limitation hampers its practicality when there is a substantial domain gap between training and open world scenes. The observed limitations motivate future research to explore how to further enhance the applicability of 3D detection models in open world scenarios by focusing on unknown instance localization and domain adaptation techniques for better model generalization.

7 Declarations

Data Availability Statement:

The data that support the findings of this study are openly available.

(1) KITTI Dataset (Geiger et al 2012): access link ², publication DOI ³.

(2) nuScenes Dataset (Caesar et al 2020): access link ⁴, publication DOI ⁵.

(3) Waymo Open Dataset (Sun et al 2020) : access link ⁶, publication DOI ⁷.

This open-sourced repository ⁸ includes all the implementation code and experimental configurations of this work.

References

- Aghdam HH, Gonzalez-Garcia A, Weijer Jvd, Lopez AM (2019) Active learning for deep detection neural networks. In: Proc. International Conference on Computer Vision (ICCV), pp 3672–3680 ⁵
- Ahmed SM, Tan YZ, Chew C, Mamun AA, Wong FS (2018) Edge and corner detection for unorganized 3d point clouds with application to robotic welding. In: Proc. International Conference on Intelligent Robots and Systems (IROS), pp 7350–7355 ¹
- Al-Saffar A, Bialkowski A, Baktashmotlagh M, Trakic A, Guo L, Abbosh AM (2021) Closing the gap of simulation to reality in electromagnetic imaging of brain strokes via deep neural networks. IEEE Transactions on Computational Imaging 7:13–21 ⁵
- Aodha OM, Campbell NDF, Kautz J, Brostow GJ (2014) Hierarchical subquery evaluation for active learning on a graph. In: Proc. IEEE Conference on Computer Vision and Pattern Recognition (CVPR), pp 564–571 ⁴
- Ash JT, Zhang C, Krishnamurthy A, Langford J, Agarwal A (2020) Deep batch active learning by diverse, uncertain gradient lower bounds. In: Proc. International Conference on Learning Representations (ICLR) ^{2, 4, 13, 14}
- Ash JT, Goel S, Krishnamurthy A, Kakade SM (2021) Gone fishing: Neural active learning with fisher embeddings. In: Proc. Annual Conference on Neural Information Processing (NeurIPS), pp 8927–8939 ^{13, 14}
- Beluch WH, Genewein T, Nürnberger A, Köhler JM (2018) The power of ensembles for active learning in image classification. In: Proc. IEEE Conference on Computer Vision and Pattern Recognition (CVPR), pp 9368–9377 ^{2, 5}
- Ben-David S, Blitzer J, Crammer K, Kulesza A, Pereira F, Vaughan JW (2010) A theory of learning from different domains. Journal of Machine Learning 79(1-2):151–175 ⁶
- Bhatnagar S, Goyal S, Tank D, Sethi A (2021) PAL : Pretext-based active learning. In: Proc. British Machine Vision Conference (BMVC), BMVA Press, p 195 ⁴
- Caesar H, Bankiti V, Lang AH, Vora S, Liong VE, Xu Q, Krishnan A, Pan Y, Baldan G, Beijbom O (2020) nuscenes: A multimodal dataset for autonomous driving. In: Proc. IEEE Conference on Computer Vision and Pattern Recognition (CVPR), pp 11618–11628 ^{12, 21}
- Caramalau R, Bhattarai B, Kim T (2021) Sequential graph convolutional network for active learning. In: Proc. IEEE Conference on Computer Vision and Pattern Recognition (CVPR), pp 9583–9592 ²
- Chen Z, Luo Y, Wang Z, Baktashmotlagh M, Huang Z (2023) Revisiting domain-adaptive 3d object detection by reliable, diverse and class-balanced pseudo-labeling. In: Proc. International Conference on Computer Vision (ICCV), pp 3714–3726 ¹
- Choi J, Elezi I, Lee H, Farabet C, Alvarez JM (2021) Active learning for deep object detection via probabilistic model-

² <https://www.cvlibs.net/datasets/kitti/>

³ <http://doi.org/10.1109/CVPR.2012.6248074>

⁴ <https://www.nuscenes.org/>

⁵ <http://doi.org/10.1109/CVPR42600.2020.01164>

⁶ <https://waymo.com/open/>

⁷ <http://doi.org/10.1109/CVPR42600.2020.00252>

⁸ <https://github.com/Luoyadan/CRB-active-3Ddet>

- ing. In: Proc. International Conference on Computer Vision (ICCV), pp 10244–10253 [2](#), [5](#)
- Citovsky G, DeSalvo G, Gentile C, Karydas L, Rajagopalan A, Rostamizadeh A, Kumar S (2021) Batch active learning at scale. In: Proc. Annual Conference on Neural Information Processing (NeurIPS), pp 11933–11944 [2](#), [4](#)
- Deng B, Qi CR, Najibi M, Funkhouser TA, Zhou Y, Anguelov D (2021) Revisiting 3d object detection from an egocentric perspective. In: Proc. Annual Conference on Neural Information Processing (NeurIPS), pp 26066–26079 [1](#)
- Du P, Zhao S, Chen H, Chai S, Chen H, Li C (2021) Contrastive coding for active learning under class distribution mismatch. In: Proc. International Conference on Computer Vision (ICCV), pp 8907–8916 [2](#), [4](#)
- Elhamifar E, Sapiro G, Yang AY, Sastry SS (2013) A convex optimization framework for active learning. In: Proc. International Conference on Computer Vision (ICCV), pp 209–216 [4](#)
- Feng D, Wei X, Rosenbaum L, Maki A, Dietmayer K (2019) Deep active learning for efficient training of a lidar 3d object detector. In: Proc. Intelligent Vehicles Symposium, (IV), pp 667–674 [2](#), [5](#), [14](#)
- Freund Y, Seung HS, Shamir E, Tishby N (1992) Information, prediction, and query by committee. In: Proc. Annual Conference on Neural Information Processing (NeurIPS), pp 483–490 [2](#)
- Freytag A, Rodner E, Denzler J (2014) Selecting influential examples: Active learning with expected model output changes. In: Proc. European Conference on Computer Vision (ECCV), pp 562–577 [5](#)
- Gal Y, Ghahramani Z (2016) Dropout as a bayesian approximation: Representing model uncertainty in deep learning. In: Proc. International Conference on Machine Learning (ICML), vol 48, pp 1050–1059 [2](#), [5](#)
- Gal Y, Islam R, Ghahramani Z (2017) Deep bayesian active learning with image data. In: Proc. International Conference on Machine Learning (ICML), vol 70, pp 1183–1192 [2](#)
- Gao M, Zhang Z, Yu G, Arik SÖ, Davis LS, Pfister T (2020) Consistency-based semi-supervised active learning: Towards minimizing labeling cost. In: Proc. European Conference on Computer Vision (ECCV), vol 12355, pp 510–526 [2](#)
- Geiger A, Lenz P, Urtasun R (2012) Are we ready for autonomous driving? the KITTI vision benchmark suite. In: Proc. IEEE Conference on Computer Vision and Pattern Recognition (CVPR), pp 3354–3361 [11](#), [21](#)
- Geng C, Huang SJ, Chen S (2021) Recent advances in open set recognition: A survey. *Transactions on Pattern Analysis and Machine Intelligence* 43(10):3614–3631 [12](#)
- Gudovskiy DA, Hodgkinson A, Yamaguchi T, Tsukizawa S (2020) Deep active learning for biased datasets via fisher kernel self-supervision. In: Proc. IEEE Conference on Computer Vision and Pattern Recognition (CVPR), pp 9038–9046 [2](#)
- Guo Y (2010) Active instance sampling via matrix partition. In: Proc. Annual Conference on Neural Information Processing (NeurIPS), pp 802–810 [4](#)
- Gupta A, Narayan S, Joseph KJ, Khan S, Khan FS, Shah M (2022) OW-DETR: open-world detection transformer. In: Proc. IEEE Conference on Computer Vision and Pattern Recognition (CVPR), pp 9225–9234 [5](#)
- Harakeh A, Smart M, Waslander SL (2020) Bayesod: A bayesian approach for uncertainty estimation in deep object detectors. In: Proc. International Conference on Robotics and Automation (ICRA), pp 87–93 [5](#)
- Hasan M, Roy-Chowdhury AK (2015) Context aware active learning of activity recognition models. In: Proc. International Conference on Computer Vision (ICCV), pp 4543–4551 [4](#)
- Houlsby N, Huszar F, Ghahramani Z, Lengyel M (2011) Bayesian active learning for classification and preference learning. *CoRR* abs/1112.5745 [2](#), [4](#)
- Huang C, Abdelzad V, Mannes CG, Rowe L, Therien B, Salay R, Czarnecki K, et al (2022) Out-of-distribution detection for lidar-based 3d object detection. In: International Conference on Intelligent Transportation Systems (ITSC), pp 4265–4271 [1](#)
- Huang R, Geng A, Li Y (2021) On the importance of gradients for detecting distributional shifts in the wild. In: Proc. Annual Conference on Neural Information Processing (NeurIPS), pp 677–689 [15](#)
- Joseph KJ, Khan SH, Khan FS, Balasubramanian VN (2021) Towards open world object detection. In: Proc. IEEE Conference on Computer Vision and Pattern Recognition (CVPR), pp 5830–5840 [1](#), [3](#), [5](#)
- Joshi AJ, Porikli F, Papanikolopoulos N (2009) Multi-class active learning for image classification. In: Proc. IEEE Conference on Computer Vision and Pattern Recognition (CVPR), pp 2372–2379 [4](#)
- Kao C, Lee T, Sen P, Liu M (2018) Localization-aware active learning for object detection. In: Proc. Asian Conference on Computer (ACCV), pp 506–522 [5](#), [14](#)
- Kifer D, Ben-David S, Gehrke J (2004) Detecting change in data streams. In: (e)Proceedings of International Conference on Very Large Data Bases ((VLDB), Morgan Kaufmann, pp 180–191 [7](#)
- Kim K, Park D, Kim KI, Chun SY (2021a) Task-aware variational adversarial active learning. In: Proc. IEEE Conference on Computer Vision and Pattern Recognition (CVPR), pp 8166–8175 [2](#), [4](#)
- Kim Y, Song K, Jang J, Moon I (2021b) LADA: look-ahead data acquisition via augmentation for deep active learning. In: Proc. Annual Conference on Neural Information Processing (NeurIPS), pp 22919–22930 [2](#), [4](#)
- Kirsch A, van Amersfoort J, Gal Y (2019) Batchbald: Efficient and diverse batch acquisition for deep bayesian active learning. In: Proc. Annual Conference on Neural Information Processing (NeurIPS), pp 7024–7035 [2](#), [4](#)
- Lewis DD, Catlett J (1994) Heterogeneous uncertainty sampling for supervised learning. In: Proc. International Conference on Machine Learning (ICML), pp 148–156 [4](#)
- Li H, Yin Z (2020) Attention, suggestion and annotation: A deep active learning framework for biomedical image segmentation. In: Martel AL, Abolmaesumi P, Stoyanov D, Mateus D, Zuluaga MA, Zhou SK, Racoceanu D, Joskowicz L (eds) Proc. Medical Image Computing and Computer Assisted Intervention (MICCAI), vol 12261, pp 3–13 [5](#)
- Liu W, Wang X, Owens J, Li Y (2020) Energy-based out-of-distribution detection. *Advances in neural information processing systems* 33:21464–21475 [15](#)
- Liu Z, Ding H, Zhong H, Li W, Dai J, He C (2021) Influence selection for active learning. In: Proc. International Conference on Computer Vision (ICCV), pp 9254–9263 [2](#), [4](#)
- Luo Y, Chen Z, Fang Z, Zhang Z, Baktashmotlagh M, Huang Z (2023a) Kecor: Kernel coding rate maximization for active 3d object detection. In: Proc. International Conference on Computer Vision (ICCV), pp 18279–18290 [5](#)
- Luo Y, Chen Z, Wang Z, Yu X, Huang Z, Baktashmotlagh M (2023b) Exploring active 3d object detection from a generalization perspective. In: Proc. International Con-

- ference on Learning Representations (ICLR) [3](#), [4](#), [7](#), [8](#), [9](#), [13](#), [14](#), [17](#)
- Luo Y, Wang Z, Chen Z, Huang Z, Baktashmotlagh M (2023c) Source-free progressive graph learning for open-set domain adaptation. *Transactions on Pattern Analysis and Machine Intelligence* 45(9):11240–11255 [12](#)
- Ma S, Zeng Z, McDuff D, Song Y (2021) Active contrastive learning of audio-visual video representations. In: *Proc. International Conference on Learning Representations (ICLR)* [2](#)
- Ma S, Wang Y, Wei Y, Fan J, Li TH, Liu H, Lv F (2023a) CAT: localization and identification cascade detection transformer for open-world object detection. In: *Proc. IEEE Conference on Computer Vision and Pattern Recognition (CVPR)*, pp 19681–19690 [6](#)
- Ma Y, Li H, Zhang Z, Guo J, Zhang S, Gong R, Liu X (2023b) Annealing-based label-transfer learning for open world object detection. In: *Proc. IEEE Conference on Computer Vision and Pattern Recognition (CVPR)*, pp 11454–11463 [2](#), [5](#)
- Maaz M, Rasheed HA, Khan S, Khan FS, Anwer RM, Yang M (2022) Class-agnostic object detection with multi-modal transformer. In: *Proc. European Conference on Computer Vision (ECCV)*, pp 512–531 [2](#), [5](#)
- MacKay DJC (1992) Information-based objective functions for active data selection. *Journal of Neural Computation* 4(4):590–604 [2](#), [4](#)
- Malinin A, Gales M (2018) Predictive uncertainty estimation via prior networks. *Proc Annual Conference on Neural Information Processing (NeurIPS)* [10](#)
- Mansour Y, Mohri M, Rostamizadeh A (2009) Domain adaptation: Learning bounds and algorithms. In: *Proc. Conference on Learning Theory (COLT)* [6](#)
- Ming Y, Sun Y, Dia O, Li Y (2023) How to exploit hyperspherical embeddings for out-of-distribution detection? In: *Proc. International Conference on Learning Representations (ICLR)* [15](#)
- Montes HA, Louedec JL, Cielniak G, Duckett T (2020) Real-time detection of broccoli crops in 3d point clouds for autonomous robotic harvesting. In: *Proc. International Conference on Intelligent Robots and Systems (IROS)*, pp 10483–10488 [1](#)
- Nguyen HT, Smeulders AWM (2004) Active learning using pre-clustering. In: Brodley CE (ed) *Proc. International Conference on Machine Learning (ICML)* [2](#), [4](#)
- Oberman AM, Calder J (2018) Lipschitz regularized deep neural networks converge and generalize. *CoRR* abs/1808.09540, [1808.09540](#) [6](#)
- Parvaneh A, Abbasnejad E, Teney D, Haffari GR, van den Hengel A, Shi JQ (2022) Active learning by feature mixing. In: *Proc. IEEE Conference on Computer Vision and Pattern Recognition (CVPR)*, pp 12237–12246 [4](#)
- Pinsler R, Gordon J, Nalisnick ET, Hernández-Lobato JM (2019) Bayesian batch active learning as sparse subset approximation. In: *Proc. Annual Conference on Neural Information Processing (NeurIPS)*, pp 6356–6367 [2](#)
- Qi J, Du J, Siniscalchi SM, Ma X, Lee C (2020) On mean absolute error for deep neural network based vector-to-vector regression. *IEEE Signal Processing Letters* 27:1485–1489 [6](#)
- Qian R, Lai X, Li X (2022) 3d object detection for autonomous driving: A survey. *Pattern Recognition* 130:108796 [1](#)
- Ren P, Xiao Y, Chang X, Huang PY, Li Z, Gupta BB, Chen X, Wang X (2021) A survey of deep active learning. *ACM Computing Survey* 54(9):40 [4](#)
- Roth D, Small K (2006) Margin-based active learning for structured output spaces. In: *Proc. European Conference on Machine Learning (ECML)*, pp 413–424 [4](#)
- Roy N, McCallum A (2001a) Toward optimal active learning through monte carlo estimation of error reduction. In: *Proc. International Conference on Machine Learning (ICML)*, pp 441–448 [5](#)
- Roy N, McCallum A (2001b) Toward optimal active learning through sampling estimation of error reduction. In: *Proc. International Conference on Machine Learning (ICML)*, pp 441–448 [2](#)
- Roy S, Unmesh A, Namboodiri VP (2018) Deep active learning for object detection. In: *Proc. British Machine Vision Conference (BMVC)*, p 91 [5](#)
- Scheirer WJ, de Rezende Rocha A, Sapkota A, Boult TE (2013) Toward open set recognition. *Transactions on Pattern Analysis and Machine Intelligence* 35(7):1757–1772 [12](#)
- Schmidt S, Rao Q, Tatsch J, Knoll AC (2020) Advanced active learning strategies for object detection. In: *Proc. Intelligent Vehicles Symposium, (IV)*, pp 871–876 [2](#), [5](#), [14](#)
- Sener O, Savarese S (2018) Active learning for convolutional neural networks: A core-set approach. In: *Proc. International Conference on Learning Representations (ICLR)* [2](#), [4](#), [7](#), [13](#), [14](#)
- Settles B, Craven M, Ray S (2007) Multiple-instance active learning. In: *Proc. Annual Conference on Neural Information Processing (NeurIPS)*, pp 1289–1296 [5](#)
- Shannon CE (1948) A mathematical theory of communication. *The Bell System Technical Journal* 27(3):379–423 [2](#)
- Shi F, Li Y (2019) Rapid performance gain through active model reuse. In: *Proc. International Joint Conference on Artificial Intelligence (IJCAI)*, pp 3404–3410 [2](#)
- Shi S, Wang X, Li H (2019) Pointcnn: 3d object proposal generation and detection from point cloud. In: *Proc. IEEE Conference on Computer Vision and Pattern Recognition (CVPR)*, Computer Vision Foundation / IEEE, pp 770–779 [6](#)
- Shi S, Guo C, Jiang L, Wang Z, Shi J, Wang X, Li H (2020) PV-RCNN: point-voxel feature set abstraction for 3d object detection. In: *Proc. IEEE Conference on Computer Vision and Pattern Recognition (CVPR)*, pp 10526–10535 [6](#), [11](#), [13](#)
- Shi W, Yu Q (2019) Integrating bayesian and discriminative sparse kernel machines for multi-class active learning. In: *Proc. Annual Conference on Neural Information Processing (NeurIPS)*, pp 2282–2291 [2](#)
- Siddiqui Y, Valentin J, Nießner M (2020) Viewal: Active learning with viewpoint entropy for semantic segmentation. In: *Proc. IEEE Conference on Computer Vision and Pattern Recognition (CVPR)*, pp 9430–9440 [2](#), [5](#)
- Sinha S, Ebrahimi S, Darrell T (2019) Variational adversarial active learning. In: *Proc. International Conference on Computer Vision (ICCV)*, pp 5971–5980 [2](#)
- Song S, Lichtenberg SP, Xiao J (2015) SUN RGB-D: A RGB-D scene understanding benchmark suite. In: *Proc. IEEE Conference on Computer Vision and Pattern Recognition (CVPR)*, pp 567–576 [2](#)
- Sun P, Kretschmar H, Dotiwala X, Chouard A, Patnaik V, Tsui P, Guo J, Zhou Y, Chai Y, Caine B, Vasudevan V, Han W, Ngiam J, Zhao H, Timofeev A, Ettinger S, Krivokon M, Gao A, Joshi A, Zhang Y, Shlens J, Chen Z, Anguelov D (2020) Scalability in perception for autonomous driving: Waymo open dataset. In: *Proc. IEEE Conference on Computer Vision and Pattern Recognition (CVPR)*, pp 2443–2451 [11](#), [12](#), [21](#)

- Tang F, Jiang C, Wei D, Xu H, Zhang A, Zhang W, Lu H, Xu C (2021a) Towards dynamic and scalable active learning with neural architecture adaption for object detection. In: Proc. British Machine Vision Conference (BMVC) 5
- Tang YP, Wei XS, Zhao B, Huang SJ (2021b) Qbox: Partial transfer learning with active querying for object detection. *Journal of IEEE Transactions on Neural Networks and Learning Systems* pp 1–13, DOI 10.1109/TNNLS.2021.3111621 2, 5
- Tran T, Do T, Reid ID, Carneiro G (2019) Bayesian generative active deep learning. In: Proc. International Conference on Machine Learning (ICML), vol 97, pp 6295–6304 2
- Van Amersfoort J, Smith L, Teh YW, Gal Y (2020) Uncertainty estimation using a single deep deterministic neural network. In: Proc. International Conference on Machine Learning (ICML), pp 9690–9700 10
- Vo HV, Siméoni O, Gidaris S, Bursuc A, Pérez P, Ponce J (2022) Active learning strategies for weakly-supervised object detection. In: Proc. European Conference on Computer Vision (ECCV), pp 211–230 5
- Wang D, Shang Y (2014) A new active labeling method for deep learning. In: Proc. International Joint Conference on Neural Networks (IJCNN), pp 112–119 4, 5, 13
- Wang J, Lan S, Gao M, Davis LS (2020) Infofocus: 3d object detection for autonomous driving with dynamic information modeling. In: Proc. European Conference on Computer Vision (ECCV), pp 405–420 1
- Wang K, Zhang D, Li Y, Zhang R, Lin L (2017) Cost-effective active learning for deep image classification. *Journal of IEEE Transactions on Circuits and Systems for Video Technology* 27(12):2591–2600 2
- Wang L, Li R, Sun J, Liu X, Zhao L, Seah HS, Quah CK, Tandianus B (2019) Multi-view fusion-based 3d object detection for robot indoor scene perception. *Sensors* 19(19):4092 1
- Wang X, Xiang X, Zhang B, Liu X, Zheng J, Hu Q (2022) Weakly supervised object detection based on active learning. *Journal of Neural Processing Letters* pp 1–15 2, 5
- Wu J, Chen J, Huang D (2022a) Entropy-based active learning for object detection with progressive diversity constraint. In: Proc. IEEE Conference on Computer Vision and Pattern Recognition (CVPR), IEEE, pp 9387–9396 2, 5
- Wu Y, Zhao X, Ma Y, Wang D, Liu X (2022b) Two-branch objectness-centric open world detection. In: Proc. International Conference on Multimedia (MM), pp 35–40 2, 5
- Yan Y, Mao Y, Li B (2018) Second: Sparsely embedded convolutional detection. *Sensors* 18(10):3337 13
- Yang Y, Ma Z, Nie F, Chang X, Hauptmann AG (2015) Multi-class active learning by uncertainty sampling with diversity maximization. *International Journal of Computer Vision* 113:113–127 4
- Yang Z, Sun Y, Liu S, Shen X, Jia J (2019) STD: sparse-to-dense 3d object detector for point cloud. In: Proc. IEEE Conference on Computer Vision and Pattern Recognition (CVPR), pp 1951–1960 6
- Yang Z, Sun Y, Liu S, Jia J (2020) 3dssd: Point-based 3d single stage object detector. In: Proc. IEEE Conference on Computer Vision and Pattern Recognition (CVPR), Computer Vision Foundation / IEEE, pp 11037–11045 6
- Yoo D, Kweon IS (2019) Learning loss for active learning. In: Proc. IEEE Conference on Computer Vision and Pattern Recognition (CVPR), pp 93–102 2, 5, 13, 14
- Yu J, Ma L, Li Z, Peng Y, Xie S (2022) Open-world object detection via discriminative class prototype learning. In: International Conference on Image Processing (ICIP), pp 626–630 2, 5
- Yuan T, Wan F, Fu M, Liu J, Xu S, Ji X, Ye Q (2021) Multiple instance active learning for object detection. In: Proc. IEEE Conference on Computer Vision and Pattern Recognition (CVPR), pp 5330–5339 2
- Zhang B, Li L, Yang S, Wang S, Zha Z, Huang Q (2020) State-relabeling adversarial active learning. In: Proc. IEEE Conference on Computer Vision and Pattern Recognition (CVPR), pp 8753–8762 2
- Zohar O, Wang K, Yeung S (2023) PROB: probabilistic objectness for open world object detection. In: Proc. IEEE Conference on Computer Vision and Pattern Recognition (CVPR), pp 11444–11453 6, 10, 15